Journal of Sedimentary Research

Journal of Sedimentary Research, 2018, v. 88, 1076–1095
Research Article
DOI: http://dx.doi.org/10.2110/jsr.2018.45

CLASTIC PIPES AND SOFT-SEDIMENT DEFORMATION OF THE JURASSIC CARMEL FORMATION, SOUTHERN UTAH, U.S.A.: IMPLICATIONS FOR PIPE FORMATION MECHANISMS AND HOST-ROCK CONTROLS

DAVID FAIRCHILD WHEATLEY* AND MARJORIE ANN CHAN
Department of Geology and Geophysics, University of Utah, 115 S 1460 E, Room 383, Salt Lake City, Utah 84112, U.S.A.
e-mail: davidfwheatley@gmail.com

ABSTRACT: **Vertically oriented columns of sandstone, termed clastic pipes, are common in Jurassic deposits of the Colorado Plateau. Exposures in the sabkha to fluvial strata of the Carmel Formation in southern Utah provide an excellent opportunity to understand pipe-formation mechanisms and controls on their expressions. These clastic pipes demonstrate significant variability and fall into two major categories: (1) primary textural pipes and (2) non-textural pipes. Primary textural pipes show significant textural differences relative to the host rock, including an internal outward grain coarsening indicative of traction structures. The pipes contain entrained, brecciated host material, and the surrounding host rock has associated soft-sediment deformation. Primary textural pipes formed through multiple liquefaction and fluidization events as evident from crosscutting pipes, multiple eruption horizons, traction structures, and other evidence of fluid-suspended-sediment transport. Non-textural pipes do not have significant textural differences from the surrounding host rock but have clear diagenetic differences (e.g., mineral coloration and cement differences) relative to the host rock. These non-textural pipes formed through the upward expulsion of fluids similar to primary textural pipes, but the fluid forces were likely insufficient to fully fluidize the sand. Overall, the porous, sandstone host rock plays a key role in explaining pipe characteristics, including their cylindrical geometry (versus tabular geometries in mudstones) and diagenetic expression. Pipe variability typically corresponds to lithologic and stratigraphic changes in the surrounding host rock. These pipe examples are key paleoenvironmental indicators, which give valuable information about subsurface fluids and the presence of a near-surface groundwater system.**

INTRODUCTION

Clastic pipes are cylindrical columns of sandstone, which vertically crosscut original bedding with sharp contacts. They typically display some level of diagenetic or textural contrast from the host rock, which results in differences in either coloration or relief. The Colorado Plateau provides some of the best examples of clastic pipes hosted in continental deposits (Hannum 1980; Hunter et al. 1992; Alvarez et al. 1998; Chan et al. 2007; Loope et al. 2013; Ross et al. 2014; Wheatley et al. 2016). Although pipes are common in the stratigraphic record, poor exposure (i.e., a lack of top and basal contacts and 3D relationships) has limited understanding of pipe formation processes and controls. In order to better understand the significance of clastic pipes, this study focuses on the Jurassic Carmel Formation, where thousands of columnar pipes vertically crosscut bedding and weather out in positive relief (Fig. 1). The high pipe density, excellent 2-D and 3-D exposures, and the variety of pipe expressions makes the area in and around the southern part of the Grand Staircase–Escalante National Monument an ideal site for characterization. The purpose of this study is to understand how various physical characteristics can indicate specific formation conditions, triggering mechanisms, controlling factors, environmental parameters, event frequency, and timing.

* Present Address: Chevron Corporation, 1500 Louisiana Street, Houston, Texas 77004, U.S.A.

PREVIOUS WORK

Injectites, including clastic pipes and dikes, have been documented in ancient deposits worldwide, including studies in California (Sherry et al. 2012), Namibia (Moss and Cartwright 2010), Patagonia (Hubbard et al. 2007), the Mediterranean (Frey-Martınez et al. 2007), and the North Sea (Duranti and Hurst 2004). Scientists have posed multiple hypotheses for the mechanism of pipe formation, including liquefaction from earthquakes (Obermeier 1996) or meteorite impacts (Alvarez et al. 1998), cold-water springs (Hannum 1980; Guhman and Pederson 1992; Draganits et al. 2003), gypsum dissolution (Hunter et al. 1992), groundwater movement (Dubiel et al. 2014), and dewatering (Phoenix 1958).

Pipes are commonly categorized within a broader suite of soft-sediment deformation (SSD) features called injectites, which includes pipes, dikes, sills, and irregular sand bodies (Hurst et al. 2011). Typically, studies of injectites have focused on mudstone-dominated, deepwater systems with particular emphasis on their petroleum application, where pipes act as fluid conduits in the subsurface (Huuse and Mickelson 2004). However, more recent studies have concentrated on the presence of pipes in continental deposits particularly in the Colorado Plateau (Chan et al. 2007; Wheatley et al. 2016). The Colorado Plateau pipes most commonly occur in the Jurassic eolian Entrada Sandstone and the sabkha Carmel Formation (Wheatley et al. 2016). Several studies document large (> 10 m in diameter) "mega-pipes" (Netoff and Shroba 2001; Netoff 2002) . Large

Published Online: September 2018

FIG. 1.—Thousands of clastic pipes in the Jurassic Carmel Formation weather out in positive relief (similar to this outcrop) in the washes and canyons of southern Utah east of the Paria River and south of HWY 89 (modified from Wheatley et al. 2016).

pipes crop out in the Jurassic Entrada Sandstone around Lake Powell (~ 100 m pipe diameter) and in the Jurassic Carmel and Entrada formations around Kodachrome basin (~ 10 m pipe diameter) (Baer and Steed 2010; Ross et al. 2014).

Previous work by Wheatley et al. (2016) examined the broad-scale spatial relationships between pipes on the Colorado Plateau and large-scale facies trends. Middle Jurassic-age pipes follow a SW to NE trend from the Arizona–Utah border to Moab, Utah paralleling the Middle Jurassic Sundance Sea. These pipes formed preferentially in the "soupy," sabkha sediments that rimmed the Sundance Sea. Additionally, they document the relationship between pipe localities and potential pipe-forming triggers. Pipe localities in the Colorado Plateau occur either in between or on the flanks of basement-cored uplifts (i.e., buried basement fault systems). Although seismic activity from the Cordilleran margin to the west could have generated the energy necessary to form pipes at some localities in the pipe trend, those earthquakes would be less likely to form pipes at other, more distant localities such as Moab, Utah (see work by Obermeier 1996 for relationships between earthquake magnitude and pipe-formation distance). Basement-cored uplifts are a more likely seismic source for pipe formation. The spatial relationship between the basement structures, thinning of Jurassic strata onto paleohighs above these structures, and beheaded folds all indicate reactivation of the basement-cored uplifts during the Middle Jurassic.

This study builds upon this previous work but focuses specifically on the smaller (< 10 m) and more numerous (thousands) pipes in the sandstone-dominated deposits of the Carmel Formation. Here, the dense occurrences of sandstone pipes provide significant data across a wide range of pipe morphologies and crosscutting relationships. Furthermore, the sabkha environment of the Carmel Formation host rock allows for further understanding of ideal pipe-forming environments, especially the role of a high water table.

STUDY AREA

A high concentration of clastic pipes crop out on a 13 km × 6.5 km exposure that forms a bench flanked on the western side by the Paria River (Fig. 2). The outcrop bench is part of the Grand Staircase sedimentary sequence present in Grand Staircase–Escalante National Monument (at the time of this research) and the surrounding state and federal land. This project has three sites on the western part of the bench roughly parallel to the Paria River, chosen based on exposure, accessibility, and pipe density.

GEOLOGIC SETTING

Stratigraphically, pipes are exposed in the Middle Jurassic Carmel Formation in the study area. The Carmel Formation has five members; in ascending order they are: (1) the fluvial Judd Hollow, (2) the eolian Thousand Pockets, (3) the fluvial Crystal Creek, (4) the interbedded sabkha coastal plain and fluvial deposits of the Paria River, and (5) the fluvial Winsor (Fig. 3). The pipes crop out almost exclusively in the Paria River Member. The Carmel Formation lies on top of the Temple Cap and Navajo formations and below the Entrada Formation. It should be noted that this study uses the Utah Geological Survey nomenclature for the Carmel Formation (Doelling et al. 2013), although other studies attribute the Thousand Pockets Tongue as part of the Page Sandstone (Blakey et al. 1983; Peterson 1994; Jones and Blakey 1997; Dickinson et al. 2010). The entire section is part of the Jurassic shallow marine to dryland depositional system, which represents the transgression and regression of the epicontinental Sundance Sea and the migration of vast dune complexes (Blakey 1994).

$^{40}Ar/^{39}Ar$ dating of multiple ash beds in the Carmel Formation provide upper and lower constraints on the age of the pipe-bearing strata and enable correlations of the section to regional events and features. The lower ash bed in the Crystal Creek Member dates to 166 Ma (Kowallis et al. 2001; Dickinson et al. 2010; Sprinkel et al. 2011) and almost directly underlies the ~ 30 m SSD interval of interest (see Stratigraphic Relationships). The upper ash bed ~ 5 m above the SSD interval in the Winsor Member dates to 164 Ma (Kowallis et al., in prep). The volcanic clasts present in the conglomerate beds of the Carmel Formation have dates of 171 Ma (Kowallis et al., in prep) and thus formed before the deposition of the Carmel Formation.

METHODS

Field methods include quantitative measurements concentrated at three field sites and qualitative observations across the outcrop bench of the study area (Fig. 2). Bed-scale stratigraphic sections were measured at each site and at several intermediate locations. Thickness, grain size, color, sedimentary structures, stratigraphic architecture, diagenetic characteris-

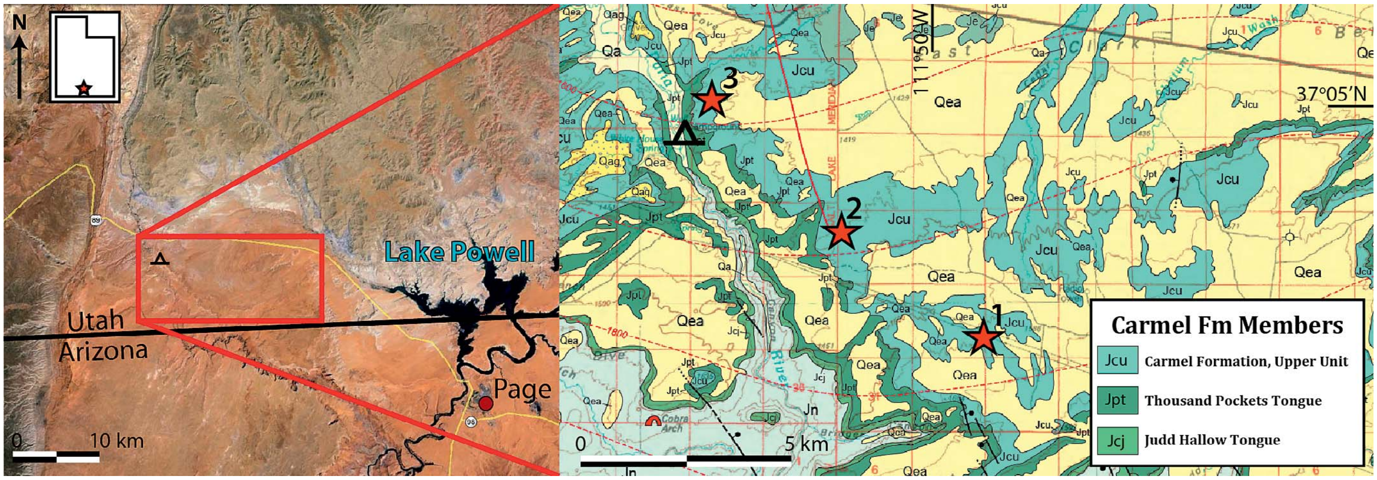

FIG. 2.—The three study sites are located in exposures of the Jurassic Carmel Formation along the western margin of a 13 km × 6.5 km outcrop bench near White House campground (black tent symbol), southern Utah (geologic map from Doelling and Willis 2006).

tics, and relationship to pipe occurrences were recorded for each bed (if applicable). Coloration names used in this study correspond to standardized Munsell color chart rock/sediment colors (Munsell soil color charts 2000). After collecting the stratigraphic sections, the individual beds were grouped into facies based on the dominant sedimentary structure, referred to here as lithofacies.

The pipe-characterization database of quantitative measurements (see Supplemental Material) includes differential GPS locations and important pipe measurements, including size and shape, grain and material properties, orientation in space, diagenetic or fluid-related features, and stratigraphic and crosscutting relationships. Differential GPS measurements were recorded with a Trimble 5700 GPS receiver and a Trimble Zephyr Geodetic Antenna. Pipe diameter, circumference, and height were measured with a measuring tape, and grain and textural information was visually estimated using a hand lens and grain-size card. Orientation and angle measurements were made with a Brunton compass and/or a protractor. These data along with additional qualitative observations comprise the basis for a pipe classification scheme. This classification divides pipe types based on relief, coloration (both of the pipe and relative to the host rock), the presence of breccia blocks, the preservation of original bedding, grain sorting, vertical extent and crosscutting relationships, common stratigraphic position, maximum grain size or clast size, scale (i.e., diameter), and associated host-rock SSD features.

Qualitative field observations across the outcrop bench are at a bed scale and cover lateral distances of kilometers. Field traverse data include observations of individual pipes (~ 2000 total, combined from ~ 900 with detailed measurements and ~ 1100 with field observations), pipe system elements (i.e., source, seal, host rock, and potential eruption layers), associated SSD, and the sedimentological context.

OBSERVATIONS AND INTERPRETATIONS

This section presents the field data and interpretations of: 1) stratigraphic and sedimentologic context for the pipes and 2) the characteristics and classification of the pipes themselves. The sections are ordered such that the observations precede the interpretations for both the sedimentologic context and the pipe descriptions. The stratigraphic relationships and lithofacies descriptions are followed by the depositional-environment interpretations of the facies associations. The pipe descriptions are followed by the pipe classification scheme, which outlines key characteristics, commonly associated lithofacies, and notable literature examples for each pipe type. These description and interpretation sections are followed by a discussion of how the stratigraphic and sedimentological information aid in determining pipe system elements (e.g., source, seal, host rock, and eruption horizons) and paleoenvironmental context, and how the pipe descriptions and classification aid in defining the formation processes of pipes.

Stratigraphic Relationships

Pipe occurrences begin in the lowermost bed of the sabkha to fluvial Paria River Member and continue upwards to the uppermost layer of the member, with maximum penetrations likely spanning the entire 20–25 m pipe-bearing interval (Fig. 4). Pipes do not occur within or come up through the underlying Thousand Pockets Tongue. Individual pipes crosscut bedding for 10+ m (Fig. 4). However, due to exposure and weathering, no pipes visibly crosscut the entire pipe-bearing section. Pipes flare upwards and outwards at the stratigraphically highest bed in the pipe interval and at one or two additional beds in the section (Figs. 4, 5). The pipe-bearing interval overlies the only significant fine-grained layer. Below this mudstone layer (~ 1 m thick) is an undulatory sandstone bed (~ 1 m thick) with abundant mudstone rip-up clasts and contorted or disrupted bedding. For the purposes of this study, the stratigraphic interval of interest is defined as the ~ 30 m SSD interval between the undulatory sandstone bed (i.e., roughly the base of the Crystal Creek Member) and the top flaring horizon (i.e., the top of the Paria River Member).

Lithofacies Descriptions and Facies Associations

Facies Associations.—The stratigraphic interval of interest contains 17 distinct lithofacies. The lithofacies are abbreviated to a letter(s) representing the principal lithology (S, sandstone; M, mudstone; Slt, siltstone/silty sandstone; T, tuff; C, conglomerate) followed by a subscript indicating the major distinguishing sedimentary structure (see Table 1, Fig. 6). The lithofacies are grouped into five major facies associations, which have paleoenvironmental implications for interpreting the context of pipe formation. Each facies association is composed of two to seven individual lithofacies that show close field associations, similar sedimentary structures or formation processes, and/or similar compositional provenance information.

Facies Association A.—Facies association A is composed of grain-flow (S_{gf}) and wind-ripple (S_{wr}) deposits. The grain-flow facies (S_{gf}) is a white (10R 9/0), crossbedded, fine- to medium-grained sandstone. Internally, the

TABLE 1.—*Carmel Formation facies and facies associations.*

Lithofacies Name	Code	Grain Size	Major Composition	Color	Sedimentary Structures and Diagenetic Features
Grain-Flow Laminae	Sgf	Very fine to medium Sand	quartz	White (10R 9/0), occasional orange and yellow	Crossbedded, cm-scale, internally massive, wedge-shaped beds or laminae
Wind-Ripple Laminae	Swr	Very fine to medium Sand	quartz	White (10R 9/0), occasional orange and yellow	Crossbedded, mm-scale, inversely graded laminae
Mudstone	M	Clay to silt	Illite–smectite, kaolinite	Maroon (7.5R 3/6)	Laminated, fissile
Siltstone	Slt	Silt, occasionally sandy	Illite–smectite, kaolinite, quartz	Red (10R 5/8 or 4/6), white (10R 9/0), yellow (7.5YR 6/2)	Thin-bedded (1–2 cm)
Crossbedded Sandstone	Scb	Fine to coarse sand, occasional granules	quartz, feldspar, volcanic fragments	Light pink (10R 6/3 or 6/4) to tan (7.5YR 7/2 or 8/2)	Indistinct to tangential crossbedding, mm-scale graded beds of volcaniclastic granules and quartz sand
Massive Sandstone	Sm	Fine to medium sand, occasional granules	quartz, feldspar, volcanic fragments	Red (10R 5/8 or 4/6), white (10R 9/0), pink (10R 6/3 or 6/4), occasional purple (5R 6/2)	Massive
Sandstone with Mud Cracks	Smc	Fine to medium sand, clay and silt, occasional granules	quartz, feldspar, volcanic fragments, clay minerals	Red (10R 5/8 or 4/6)	Mud cracks
Sandstone with Root Casts	Src	Fine to medium sand, occasional granules	quartz, feldspar, volcanic fragments	Red (10R 5/8 or 4/6) to mottled red and white (10R 9/0)	Root casts
Tabular Conglomerate	C	Pebble to cobble, occasional boulder (≤ 2 m)	volcanic clasts, quartzite, other rock fragments	Maroon (10R 3/4)	Tabular, 20–30 cm-thick bed extending laterally for 100s of meters
Volcanic Tuff (Ash Fall)	Tva	Clay	biotite, volcanic ash	Purple (5P 4/2), green (10G 8/2)	Massive to thin-bedded (mm)
Volcaniclastic Sandstone	Svc	Very coarse sand to granule	volcanic fragments	Various	Thin-bedded (1–2 cm), Convolute to wavy bedding
Brecciated Sandstone	Sb	Fine to medium sand	quartz	White (10R 9/0)	Breccia blocks
Deformed Crossbedded Sandstone	Sdc	Fine to coarse sand, occasional granules	quartz, feldspar, volcanic fragments	Light pink (10R 6/3 or 6/4) to tan (7.5YR 7/2 or 8/2)	Deformed cross stratification
Faulted Sandstone	Sf	Fine to medium Sand	quartz, feldspar, volcanic fragments	Red (10R 5/8 or 4/6), white (10R 9/0), pink	Synsedimentary faults
Sandstone Pipe	Scp	Fine sand to Granule, occasional pebble	Quartz, feldspar, volcanic fragments	White (10R 9/0), red (10R 5/8 or 4/6)	Clastic pipes
Irregularly Injected Material and/or Irregularly Bleached Sandstone	Sib	Fine to medium sand, occasional granules	quartz, feldspar, volcanic fragments	Red (10R 5/8 or 4/6) to mottled red and white (10R 9/0)	Irregularly injected material, irregular bleaching and/or mottling
Flaring Sandstone	Sfl	Fine to medium sand, occasional granules	quartz, feldspar, volcanic fragments	Light pink (10R 6/3 or 6/4) to tan (7.5YR 7/2 or 8/2)	Pipes flare outwards
Convoluted Sandstone	Sc	Fine to coarse sand, some granules and 1–2 cm shale clasts	quartz, feldspar, volcanic fragments, clay minerals	Tan (7.5YR 7/2 or 8/2)	Convoluted bedding, shale rip-up clasts

*Orange, Facies Association A; Green, Facies Association B; Yellow, Facies Association C; Blue, Facies Association D; Purple, Facies Association E

facies is composed of centimeter-scale, internally massive, wedge-shaped beds. The wind-ripple facies (S_{wr}) is a white (10R 9/0), crossbedded, fine- to medium-grained sandstone. Internally, the facies contains mm-scale, inversely graded laminae. Both facies exhibit planar, wedge, or trough crossbedding on a scale of meters to tens of meters. In stratigraphic sections these two facies are represented as meter-scale planar-cross-bedded sandstones.

Facies Association B.—Facies association B is composed of mudstone (M), siltstone/silty sandstone (Slt), fine- to coarse-grained crossbedded sandstone (S_{cb}), and some massive sandstones (S_m). The mudstone (M) lithofacies is a maroon (7.5R 3/6), laminated mudstone. Mudstone intervals $>$ 1 m in thickness are laterally continuous over several kilometers. The siltstone (Slt) lithofacies is a red (10R 5/8 or 4/6), white (10R 9/0), or yellow (7.5YR 6/2), thin-bedded (1–2 cm) siltstone. The crossbedded sandstone (S_{cb}) lithofacies is a light pink (10R 6/3 or 6/4) or

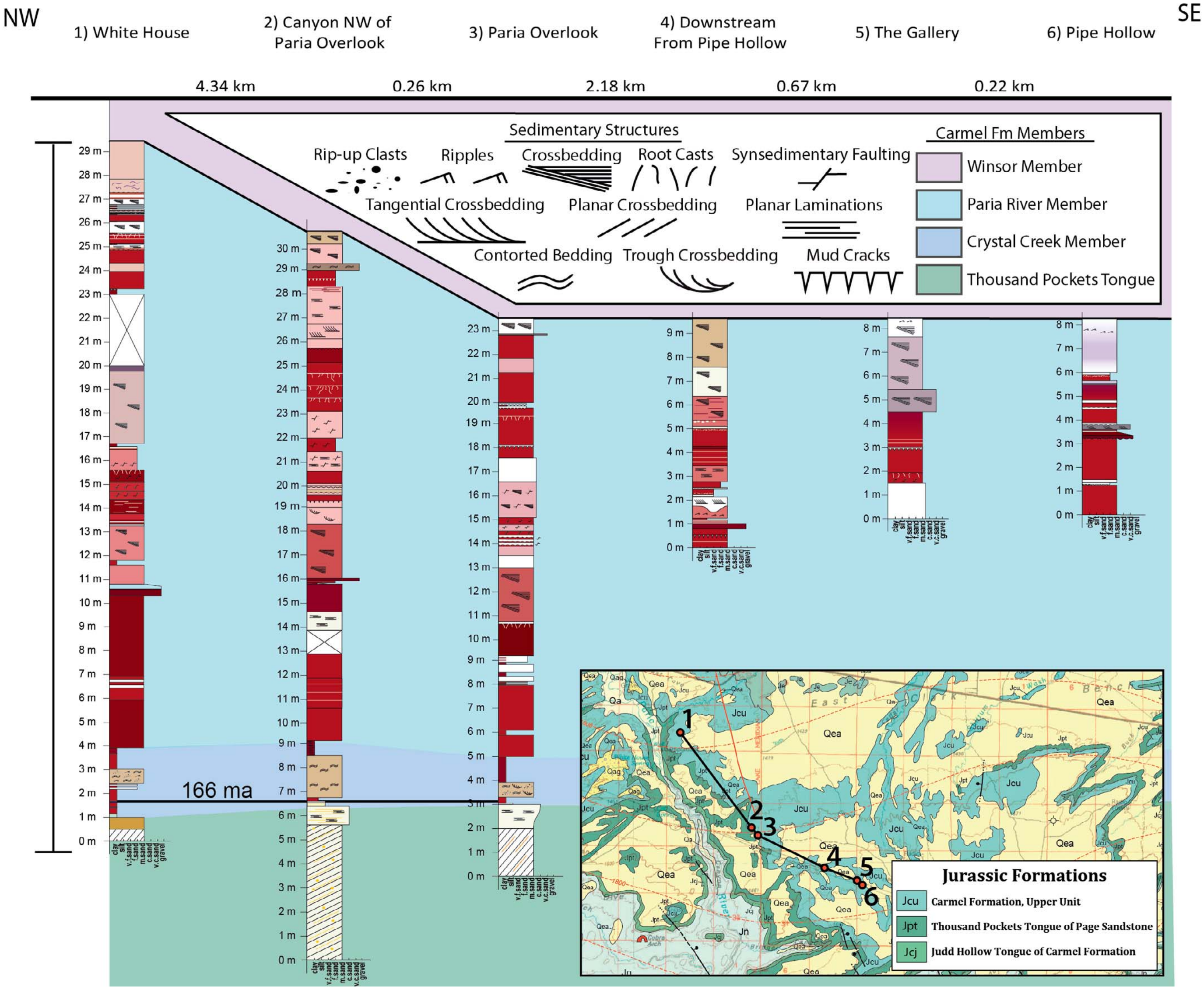

FIG. 3.—Six measured sections form a transect between the three major field sites. Clastic pipes are primarily in sabkha deposits of the Paria River Member, Carmel Formation. The sections are hung on a 166 Ma ash bed or the top of the Paria River Member when the ash bed is not present (geologic map from Doelling and Willis 2006). Note: The basal member of the Carmel Formation, the Judd Hollow Member, is not depicted on the cross section.

tan (7.5YR 7/2 or 8/2), crossbedded, fine- to coarse-grained sandstone. Granule-size material, commonly composed of volcanic fragments, occurs as a lag along the base of a crossbed set or occurs between individual laminae. For the purposes of this paper, all crossbedding with beds at the tens of centimeter scale is grouped into this facies (S_{cb}), including tangential crossbedding, trough crossbedding, and wedge crossbedding. The small (tens of centimeter) dune sets can have either flat or erosional bases and contain channel morphologies. Those with erosional bases both thicken or thin dramatically (100–200%) over lateral distances (< 100 m). Facies association B also contains the massive sandstone facies (S_m) (see below).

Facies Association C.—Facies association C is composed of massive sandstones (S_m) occasionally capped by mud cracks (S_{mc}) or root casts (S_{rc}). Facies association C is the dominant host rock for the pipes in addition to facies association B. The massive sandstone (S_m) lithofacies is a red (10R 5/8 or 4/6) (occasionally white (10R 9/0), pink (10R 6/3 or 6/4), or light purple (5R 6/2)), fine- to medium-grained massive sandstone. Typically, the beds have tabular geometries. The sandstone with mud cracks (S_{mc}) and the sandstone with root casts (S_{rc}) lithofacies is a tabular, red massive sandstone capped by either mud cracks or root casts respectively. Root cases are typically < 50 cm in length, maintain a relatively consistent diameter, and have curving or branching morphologies. However, where the root casts are > 1 m in length, they taper downwards and have a vertical orientation, resembling a "taproot" in appearance.

Facies Association D.—Facies association D is composed of tabular, laterally continuous volcanic-rich conglomerates (C), ash beds (T_{va}), and volcaniclastic sandstones (S_{vc}). The conglomerate (C) lithofacies is a maroon (10R 3/4), pebble- to cobble-size conglomerate, with occasional boulders. The beds are commonly only several tens of centimeters in thickness, tabular, and extend for several hundreds of meters. The volcanic tuff (T_{vc}) lithofacies is a purple (5P 4/2) or light green (10G 8/2) volcanic

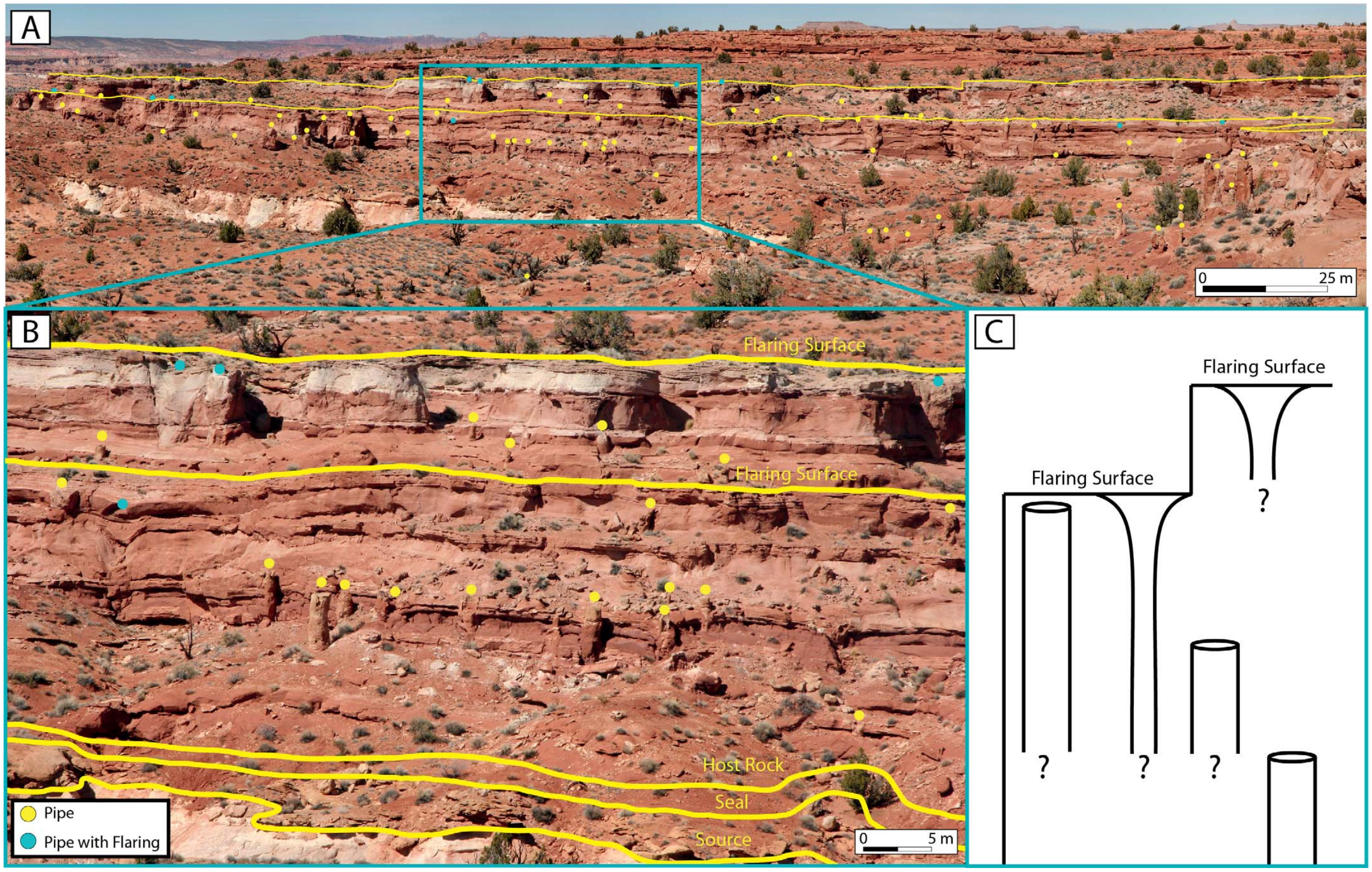

FIG. 4.—The entire pipe system (source, seal, host rock, and eruptive structures) occurs in an ~ 30 m section of the Carmel Formation. Pipe occurrences begin in the lowermost bed of the Paria River Member of the Carmel Formation and continue up to the contact between the Paria River and Winsor Members (Panel A and enlarged in Panel B). Although the top and base relationships are commonly obscured due to erosion, pipes in the right half of Panel A can be observed continuously for 10+ m. Some pipes have flaring geometries that occur at several correlative horizons in the pipe system and likely represent eruption horizons (Saucier 1989; Obermeier 1996). Panel C demonstrates the various geometries and top and base relationships of pipes observed along the photomosaic.

ash depending on the degree of alteration. Unaltered volcanic ashes have datable euhedral biotite crystals. The dated ash beds act as chronostratigraphic markers. The volcaniclastic sandstone (S_{vc}) facies is a gray (5R 6/1 or 5/1) to multicolored, thin-bedded (1–2 cm), very coarse-grained sandstone composed mainly of volcanic fragments. The volcanic clasts have sanidine, plagioclase, biotite, quartz, and several other accessory minerals surrounded by a fine-grained glassy matrix. The facies contains low-angle (< 15°) tangential to wedge crossbedding and occurs chiefly in the upper 4–6 m of the Paria River Member.

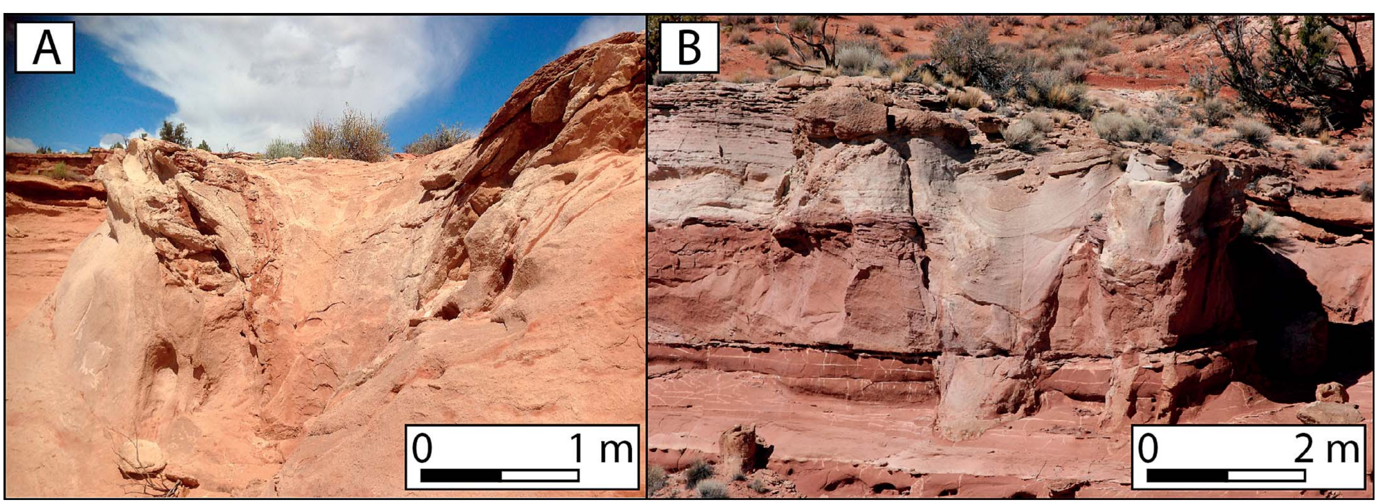

FIG. 5.—Pipes have outward-flaring geometries at several correlative horizons interpreted to be eruption horizons.

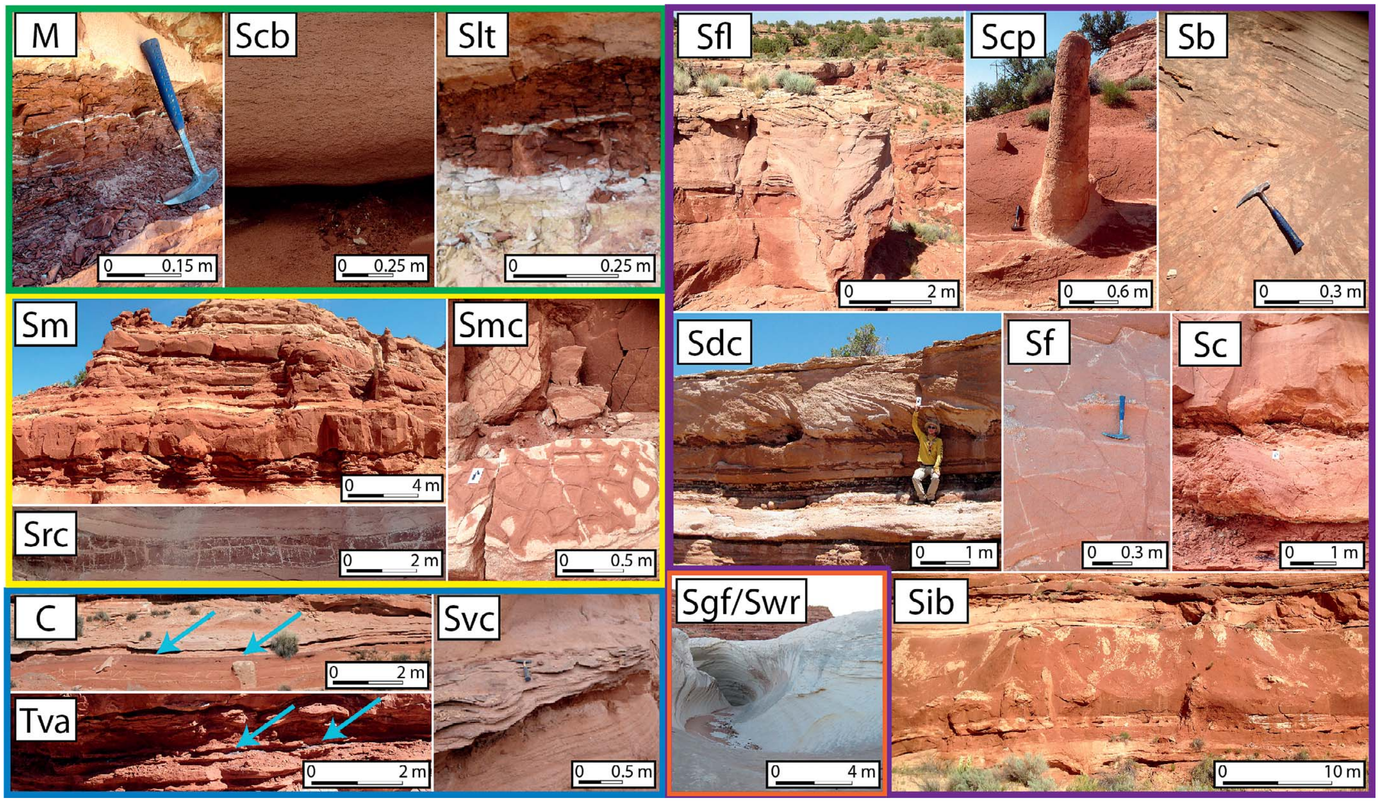

FIG. 6.—The 17 major lithofacies are separated into five facies associations (A–E), grouped into color outline boxes that are color-coded to the facies associations of Table 1 (A, orange; B, green; C, yellow; D, blue; E, purple). Lithofacies are abbreviated to a letter(s) representing the principal lithology (S, sandstone; M, mudstone; Slt, siltstone/silty sandstone; T, tuff; C, conglomerate) followed by a subscript indicating the major distinguishing sedimentary structure. (Symbol key: grain flow (S_{gf}), wind ripple (S_{wr}), mudstone (M), crossbedded sandstone (S_{cb}), siltstone/silty sandstone (Slt), massive sandstone (S_m), massive sandstone capped by mud cracks (S_{mc}), massive sandstone capped by root casts (S_{rc}), volcaniclastic sandstone (S_{vc}), ash bed (T_{va}), volcanic-rich conglomerates (C_t), brecciated sandstone (S_b), deformed crossbedded sandstone (S_{dc}), synsedimentary-faulted sandstone (S_f), sandstone clastic pipes and dikes (S_{cp}), irregular sandstone bodies or irregularly bleached sandstone (S_{ib}), flaring sandstone (S_{fl}), and convoluted sandstone (S_c)).

Facies Association E.—Facies association E is composed of brecciated sandstone (S_b), deformed crossbedded sandstone (S_{dc}), convoluted sandstone (S_c), synsedimentary-faulted sandstone (S_f), sandstone clastic pipes and dikes (S_{cp}), irregular sandstone bodies or irregularly bleached sandstone (S_{ib}), and flaring sandstone (S_{fl}). The brecciated sandstone (S_b) facies is a white (10R 9/0), synsedimentary-brecciated, fine- to medium-grained sandstone. The brecciation typically crosscuts the grain-flow (S_{gf}) and wind-ripple (S_{wr}) facies or is localized to the area in and around the sandstone pipes (S_{cp}). The deformed crossbedded (S_{dc}) facies is a light pink (10R 6/3 or 6/4) or tan (7.5YR 7/2 or 8/2), fine- to coarse-grained sandstone. The facies shows relict crossbedding that was deformed before lithification producing a "fluid-like" appearance and oversteepened slip faces. The convolute-sandstone (S_c) facies is a tan (7.5YR 7/2 or 8/2), fine- to coarse-grained sandstone with convolute or undulatory bedding and common angular mudstone clasts and typically occurs in the Crystal Creek Member (lower 4 m stratigraphic interval of interest). The faulted-sandstone (S_f) facies is a red (10R 5/8 or 4/6), white (10R 9/0), and/or pink (10R 6/3 or 6/4), faulted, fine- to medium-grained sandstone (for a more detailed description of the faulting see the section entitled Other Soft-Sediment Deformation and/or Fluid-Related Features). The irregular sandstone bodies or irregularly-bleached-sandstone (S_{ib}) facies is a mottled red (10R 5/8 or 4/6) and white (10R 9/0), fine- to medium-grained sandstone. The facies commonly occurs in discrete stratigraphic intervals typically 1–3 m in thickness. The facies is compositionally and texturally similar to the sandstone pipe facies but has irregular morphologies instead of the cylindrical shape of clastic pipes. The material surrounding and between the irregularly shaped sand bodies displays mottled bleaching with irregular geometries. The sandstone pipe (S_{cp}) facies represents the clastic pipes described in detail in this study. The facies refers to a column of fine- to medium-grained sandstone that vertically crosscuts primary bedding with sharp contacts. The flaring sandstone (S_{fl}) facies occurs only in association with the sandstone pipe facies and is both texturally and compositionally similar. The facies has a funnel-shaped morphology and "flares out" from the sandstone pipe to a bed interface. The flaring horizons correlate to two or three stratigraphic surfaces.

Facies-Association Interpretations and Depositional Environments

Here, the five major facies associations (A–E) are separated into two major groupings based on the depositional or origin interpretations of the facies. In general, the first four facies associations correspond to specific environments and include the eolian (A), fluvial (B), sabkha (C), and volcanically influenced (D) facies associations. The SSD (E) facies association occurs within and crosscuts the eolian, fluvial, sabkha, and volcanically influenced facies associations. Although the SSD facies does not represent a specific environment, the distinct textural fabrics and sedimentary structures require that this group be delineated from the surrounding facies. Each depositional facies association is composed of one to seven individual lithofacies (Table 1, Fig. 6).

Facies association A is interpreted as eolian because of the abundant wind-ripple and grain-flow laminae, meter-scale cross bedding, and appropriate textural information (i.e., very fine- to medium-grained, very well-rounded sand). Facies association B is interpreted as fluvial because of channelized, trough cross-bedded sandstones in close association with laminated mudstones. The channelized sandstones have erosional bases and flat tops, and thicken and thin laterally over short ($<$ 100 m) distances. The sandstones represent channel fill and the associated mudstones represent overbank deposits. Facies association C is interpreted as sabkha due to evidence of wetting and drying (e.g., mud cracks) as well as some degree of ground water (e.g., root casts from biologic community), and the establishment of a relatively flat stable surface in line with the interpretation of an arid coastal plain (e.g., a lack of traction structures, flat tops and bases to the beds, and root casts indicating elapsed time on a single surface). The fluvial (B) facies association commonly erodes down into the sabkha (C) facies association, indicating that the sabkha was dissected by rivers or wadis similar to modern arid coastal plains or sabkhas. Facies association D is grouped based on the abundant presence of volcanic material. The tabular, laterally continuous conglomerates are interpreted as debris flows (Chapman 1987, 1989, 1993). The volcaniclastic sandstones represent coarse- to very coarse-grained volcanic material moved through traction currents, and the volcanic ashes are deposited via air fall from a volcanic eruption. Facies association E is interpreted as the result of SSD due to highly disturbed and contorted bedding, injection features, crosscutting relationships with primary bedding and sedimentary structures, and an overall chaotic nature.

The eolian (A) facies association, mapped as the Page Sandstone or the Thousand Pockets Tongue of the Carmel Formation, underlies the pipe-bearing strata. The pipe-bearing strata include the fluvial (B) and sabkha (C) facies associations with minor ($<$ 5% by thickness) contributions from the volcanically influenced (D) facies association. Overall, the study-area stratigraphy represents a dune complex (S_{gf} and S_{wr}) overlain by an arid coastal plain sabkha. Rivers dissected the sabkha sediments and dominate the upper part of the section representing an increase in fluvial activity through time. Mud cracks (S_{mc}) occur throughout the section and indicate multiple wetting and drying events. Root casts (S_{rc}) demonstrate that the arid coastal plain did support vegetation and potentially an associated ecosystem. However, the biotic community was likely not very productive as little to no additional trace fossils and no body fossils were found in the study area.

Deposition of volcanic material, represented by facies association D, was ubiquitous throughout the interval both temporally and spatially. This includes multiple ash beds (T_{va}), volcaniclastic sandstones (S_{vc}), 10–30 cm tabular debris-flow conglomerate beds containing large volcanic cobbles (C), and volcanic clasts ranging from $\sim$ 1 mm to $\sim$ 2 m in diameter. After deposition and before burial, the region experienced extensive SSD, producing a variety of structures. The resulting SSD (E) facies association crosscut and overprinted the original depositional facies and removed many primary sedimentary structures. Overall, the sedimentological context of the host rock indicates that pipes formed preferentially in the wetter sabkha and fluvial strata. These strata would have had a greater degree of water saturation compared to other arid Middle Jurassic continental deposits.

Pipe Characteristics and Features

Pipes in the study area form in notably high densities ($>$ 500 pipes per 7500 m^2). This section summarizes the major characteristics and trends of the $\sim$ 900 pipes that were measured and studied at the three major field localities (Fig 7). These characteristics form the backbone of the quantitative data for the three field sites and the classification scheme discussed later. Many pipes possess the features outlined below; however, the majority of pipes do not possess all of these features simultaneously.

Geometry.—By definition, all pipes have a roughly cylindrical shape. The pipes in the database have diameters ranging from 0.1 to 7 m (Fig. 8), and heights ranging from 0.01 to 9 m. In general, pipes tend to maintain their cylindrical shape with only minor changes in diameter corresponding to a few degrees of vertical tapering (Fig. 8).

Orientation in Space.—Pipes have a dominantly vertical orientation; however, $\sim$ 14% of the pipes have a discernible lean or tilt towards the north (Fig. 9A). Although the lean has a consistent orientation, the pipes have no consistent tilt magnitude with respect to bedding. Less than 1% of pipes bend and twist in an upward direction such that the magnitude and direction of their lean changes throughout the vertical length of the pipe.

Material Properties.—Pipes are composed of fine- to medium-grained (rarely coarse-grained) quartz sand (80+%) with varying amounts of volcanic fragments, other lithic fragments, and feldspar grains. The quartz-rich sand "groundmass" of the pipes tends to be well rounded and well sorted. Volcanic fragments range in size from fine-grained sand to pebble size and are the second most abundant grain type in the pipes (from hand lens and petrographic estimations).

The pipes show internal radial sorting with larger grain sizes on the outer edge of the pipes. The sorting is most apparent in the volcanic and lithic fragments, which have a larger range in grain size (fine-grained sand to pebble) relative to the quartz sand (fine- to medium-grained sand). Typically the quartz grains range from upper fine-grained sand in the center to medium-grained sand on the edge. Some pipes have a gradual internal, radial sorting. However other pipes have a distinct, sharp change in grain size, creating a coarser-grained rind ranging from medium-grained sand to pebbles on the outer 1–5% of the diameter of the pipes (Deynoux et al. 1990). The outer rind typically has a greater percentage of volcanic and lithic fragments relative to the interior of the pipe, with some rinds composed almost entirely of volcanic and lithic fragments. Several of the pipes have larger entrained pieces of host rock, including angular mudstone fragments (2–5 cm in diameter) and angular blocks of red sandstone ($\sim$ 0.1–2 m in diameter) with thin (several millimeters) bleached rinds.

Diagenetic and/or Fluid-Related Features.—The pipes have several diagenetic and/or fluid-related features, including prominent carbonate rhombs (Fig. 9B) and nodules (Fig. 9C), in addition to banded cements (alternating carbonate and iron oxide layers) (Fig. 9D). The carbonate mineral masses are concentrated on the southern outside edges of the pipes (Fig. 9E), but sometimes they develop in the interior. They occur as crystals up to 1 cm in length, granular nodules (a mass of mixed carbonate and iron oxide material), or small crystal-lined vugs.

Many pipes have a distinct coarser-grained outer rind that is preferentially cemented. The preferential rind cementation results in distinctive weathering bowls or pits sometimes termed "armchair weathering" (Netoff and Shroba 2001), where the well-cemented outer edge of the pipe protrudes upwards in positive relief since it is more resistant to erosion. Correspondingly, the more weakly cemented interior part of the pipe weathers as a bowl or depression. In extreme cases, one side of the bowl may collapse, leaving a raised back and reduced sides that resemble the shape of an armchair (Fig. 9F, G). Typically one higher point along the rim will be the most resistant (commonly several centimeters to tens of centimeters); however, the maximum point does not have any consistent orientation. The variety of weathering features at this site have also been similarly documented in larger pipes in the Lake Powell region (Netoff and Shroba 2001).

In addition to their bleached color, some pipes have a well-defined bleached zone, which extends beyond the textural boundary of the pipe (Fig. 9H, I). The bleached zones are typically equidimensional and circular (occasionally asymmetrical to teardrop shaped). Some of the bleached zones resemble "paint splatter," with numerous (hundreds), of radially

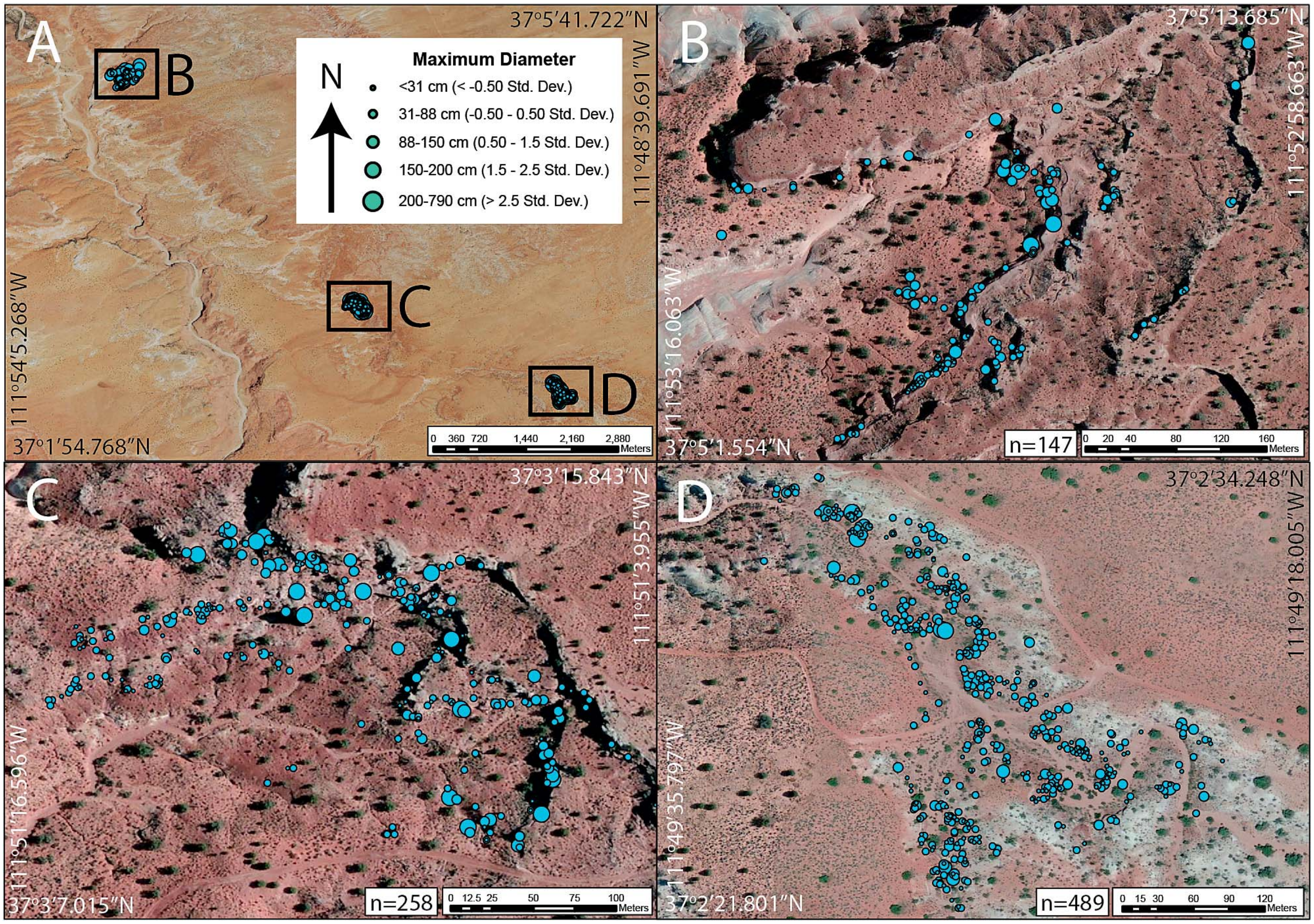

FIG. 7.—Numerous (~ 900) clastic pipes occur throughout the three separate field sites. This study cataloged ~ 45 measurements of pipe characteristics for each pipe. Pipes are displayed here as blue dots, which correspond to the pipe's relative diameter. Basemap imagery from ArcGIS 10.3 High Resolution Global Imagery (Source: Esri, DigitalGlobe, GeoEye, Earthstar Geographics, CNES/Airbus DS, USDA, USGS, AEX, Getmapping, Aerogrid, IGN, IGP, swisstopo, and the GIS User Community).

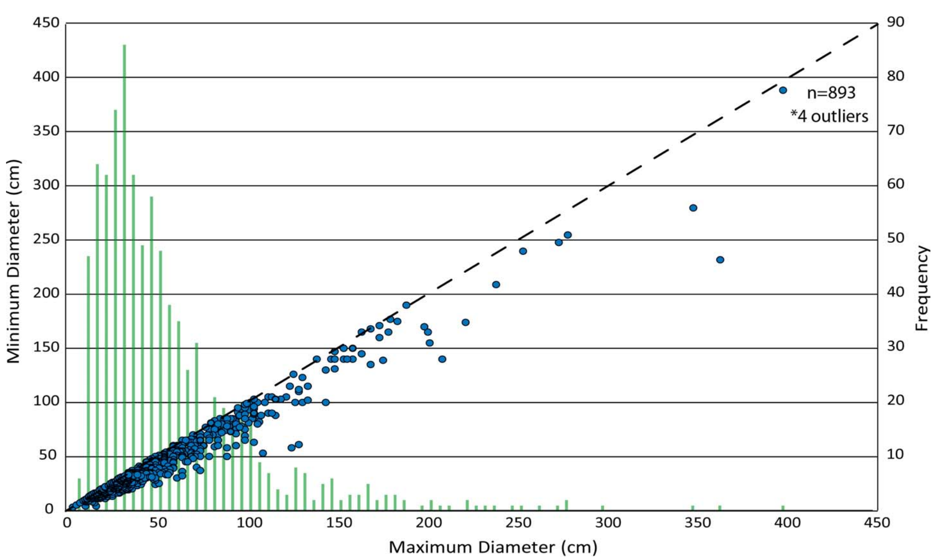

FIG. 8.—Pipe diameters generally range from ~ 10 cm to several meters with outliers up to ~ 7 m. The histogram of pipe diameters shows a positive or right-skewed distribution. The cross plot of the maximum and minimum diameter (blue dots) fall on or near the 1:1 line (dashed black line), indicating a dominantly circular geometry. Note: For display purposes the graph is truncated after 4.5 m. Four pipes have diameters greater than 4.5 m and less than approximately 7 m.

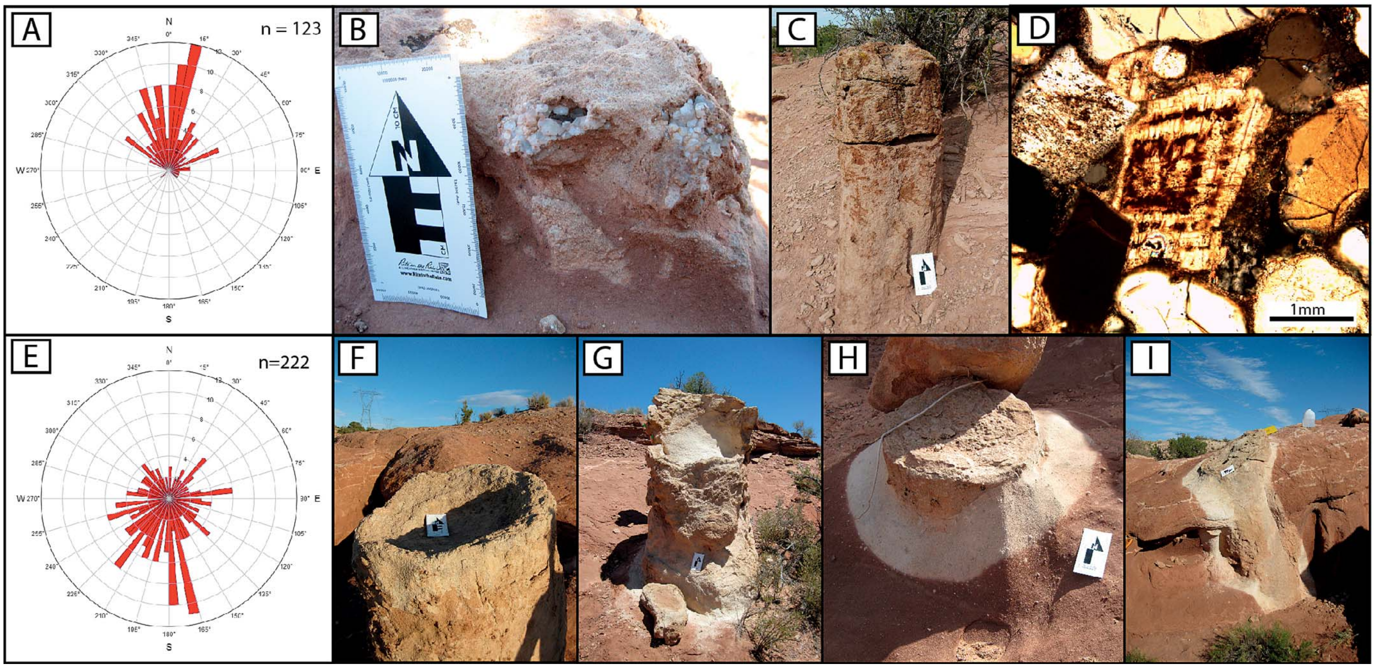

FIG. 9.—Pipes vertically crosscut bedding; however, ~ 14% of pipes have a discernible nonvertical orientation (up to ~ 32 degrees off vertical) with a consistent northern lean (Part A). Carbonate nodules occur on the outside of pipes predominantly on the southern side of pipe exposures (Part E) (opposite of the northern lean). These nodules can occur as carbonate rhombs (Part B) or as carbonate and iron oxide mineral masses (Part C). Pipes and host rock typically have iron oxide and carbonate cements, which can occur as banded cements with alternating layers (Part D). Pipes have outward coarsening often with a distinct outer rind of coarser-grained material. This outer rind is more indurated as a result of preferential cementation. As pipes erode, they form bowl-shaped depressions. When the bowl becomes too deep, one side will fall away, creating an armchair-shaped geometry (Parts F, G). Pipes are bleached white against a red (10R 5/8 or 4/6) host-rock background as a result of reducing diagenetic fluid flow through the pipes. Some pipes have a bleached halo which extends beyond the pipe and parallels the pipe geometry (circular in map view and cylindrical in 3D view) (Parts H, I). Some pipes have millimeter-scale circles that emanate beyond the bleached halo, resembling paint splatters.

positioned millimeter-scale bleached circles surrounding the pipes. The zones have diameters ranging from < 1 cm to ~ 30 cm, and the diameter of the bleached zone has no clear relationship with the diameter of the pipe.

Other Soft-Sediment Deformation and/or Fluid-Related Features

Although pipes, as defined by this study, are the most prominent SSD feature of the Carmel Formation interval, many other related SSD features occur in the pipe-bearing interval, including faults, folds and undulating bedding, irregular bleaching and mottling, dikes, irregular sandstone bodies, and brecciation. Although irregular bleaching and mottling is not a type of SSD, the bleaching in the study area is integrally linked to the SSD (e.g., follows the deformed beds and laminae, occurs exclusively in association with SSD, etc.) and was therefore included in this list. The related SSD is confined almost exclusively to the stratigraphic section where pipes are present.

Extensive synsedimentary normal, reverse, and antithetical faults occur throughout the pipe section with offsets of millimeters to meters. Some larger pipes have faults surrounding the pipe itself with a damage zone of faults extending outwards one to two times the diameter of the pipe (Fig. 10). These damage zones and the associated pipes are classified as ring-fault pipes. Some damage zones have nested scales of deformation with a prominent ring fault surrounding the outermost boundary of the damage zone and successively lesser offsets in the interior. Even with many faults directly associated with pipes, faults do not crosscut pipes.

Synsedimentary folding is less common than faulting and is confined to the lower and upper 4–6 m of the interval of interest, which represents the muddier parts of the section. Most of the folding occurs near the base of the SSD interval. The upper boundary of the ~ 4 m folded interval is a low-amplitude (~ 1 m) and long-wavelength (~ 5–10 m) fold. Internally, the interval has a greater degree of disruption with highly contorted beds, recumbent folds, and other undulatory or irregular features.

Irregular sandstone bodies have amorphous or irregular geometries typically consisting of irregular blob-like shapes roughly parallel or oblique to bedding. These are referred to as pseudo-pipes or pseudo-pipe material because of their textural and diagenetic similarity to standard pipes. Irregular sandstone bodies are stratigraphically restricted to discrete zones in association with substantial bleaching and mottling of the host rock (commonly in the massive-sandstone facies).

Extensive bleaching and mottling exists throughout the pipe section; however, several stratigraphic intervals have increased levels of bleaching. These beds also stratigraphically constrain mottled pipes and irregular sandstone bodies. The bleaching typically falls into two major categories: (1) linear bleaching, which is preferentially associated with faults or fractures, and (2) irregular and/or mottled bleaching typically associated with irregular sandstone bodies. In addition to these two main categories, bleached blobs and splotches also occur throughout the section.

Brecciation occurs almost exclusively near the bottom and top 4–6 m of the stratigraphic interval of interest. Brecciation in the lower 4 m of the section occurs in the synsedimentary folded and contorted mudstone and sandstone layer as brecciated mudstone clasts. Many of these clasts have a bleached halo or rim, and sometimes the maroon mudstone coloration (7.5R 3/6) is altered to a light purple (5R 6/2 or 5RP 6/2). In the top 6 m of the section brecciation is almost exclusively in association with pipes (typically as breccia pipes). These breccia blocks are composed of both mudstone and sandstone, with some breccia blocks as large as 2 m in diameter. Breccia blocks in the upper 6 m of the section also have bleached halos or rims.

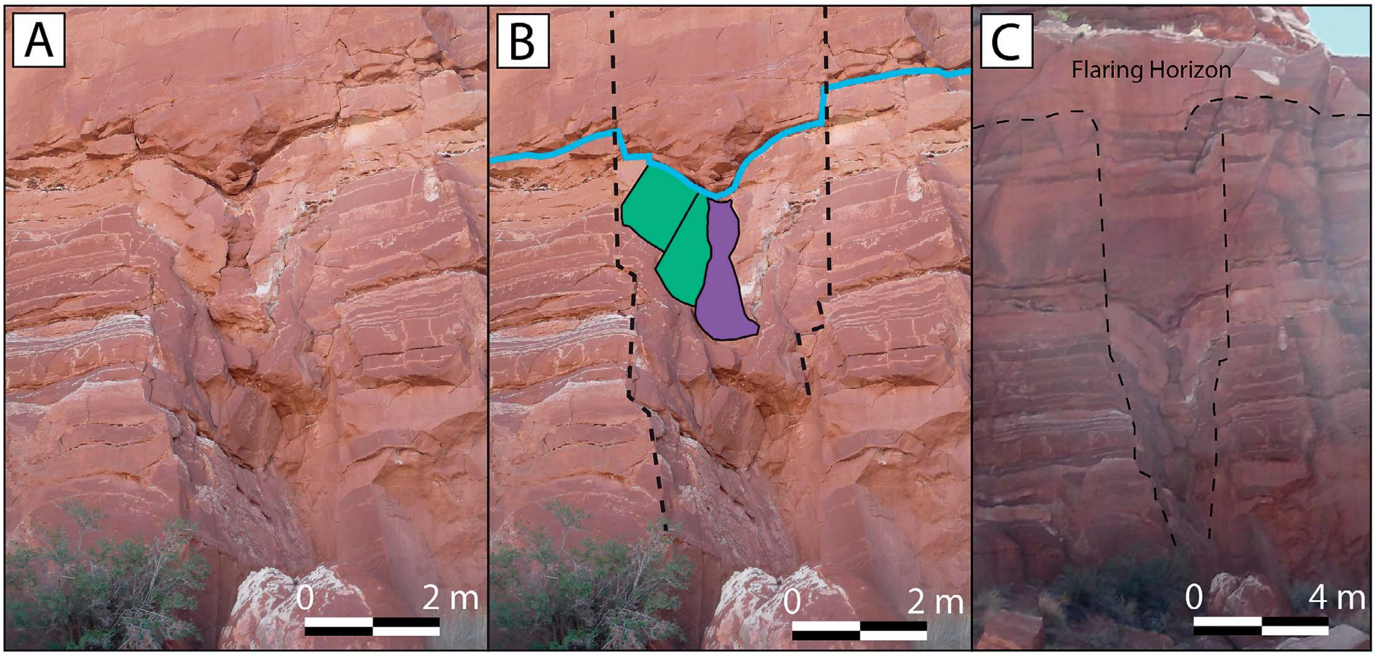

FIG. 10.—Many pipes have damage zones surrounding the pipes. These damage zones are a series of stair-stepped down-faulted grabens and can be either normal or antithetical faults (interpreted as ring faults). The structures are caused by dewatering following pipe emplacement. This pipe has nested scales in the damage zone, which is bounded by a large fault on either side of the pipe, interpreted as a ring fault (black dashed line of Part B). In the damage zone the faulted blocks (green of Part B) are rotated towards the pipe (purple of Part B), demonstrating inward collapse. Additionally, this pipe did not reach the surface, given the faulted mudstone horizon above the pipe (light blue of Part B). Evidence indicates that some pipes reached the surface while others did not. The ring fault that bounds the damage zone (black dashed lines) continues vertically and dies out in the flaring horizon (Part C). The offset in the dashed lines in Part C is due to the erosional expression of the feature.

Pipe Classification Scheme

Although all pipes have a vertical, cylindrical geometry, they display significant variability, resulting in a variety of expressions (Fig. 11). Multiple studies have documented pipes dominated by breccia blocks (Schlee 1963) to those composed of massive sandstone (Schlee 1963; Hannum 1980). Many of the pipe expressions in this field area are stratigraphically or lithologically constrained, either occurring only at certain stratigraphic levels or in certain host-rock facies. The pipes are classified into ten major pipe types using geometry, relief, coloration, coloration relative to the host rock, preservation of internal stratification, presence of host rock breccia blocks, and vertical character (Table 2). These pipe types are organized into two major groups: (1) dominantly primary textural pipes, which have properties that include grain sorting, a larger maximum grain size than the surrounding host rock, internal breccia blocks, positive relief, and/or associated synsedimentary faulting, and (2) dominantly non-textural pipes, which have no major textural differences from the host rock (Fig. 11, Table 2).

Primary Textural Pipes

Standard Pipe.—The most common type of pipe is the standard pipe, which weathers out of the host rock in positive relief (Fig. 11). It crosscuts layers vertically for 10+ m (Fig. 4), and most commonly occurs in the sabkha facies association. In particular, standard pipes at field site 3 occur in higher frequencies in the lower 6 m of the pipe-bearing section, specifically in the beds immediately above the first pipe occurrence. Standard pipes display grain-size sorting resulting in either a gradual outward coarsening or an outer rind composed of coarser material. Approximately 18% of pipes have an outer rind, which is typically composed of medium- to coarse-grained quartz sand and volcanic fragments up to pebble size. Standard pipes are bleached white (10R 9/0), in contrast to the dominantly red (10R 5/8 or 4/6) host rock, and commonly occur in the S_m, S_{mc}, and S_{rc} facies. Many studies have recorded standard pipe types across multiple field localities in Middle Jurassic strata of the Colorado Plateau including Kodachrome basin (Hannum 1980; Ross et al. 2014), Lake Powell (Netoff and Shroba 2001; Netoff 2002), and the Laguna region (San Juan Basin) of New Mexico (Schlee 1963; Hunter et al. 1992).

Breccia Pipe.—Breccia pipes contain locally derived breccia blocks and/or clasts suspended in a sandstone matrix (Fig. 11), and are most prevalent in the uppermost 4–6 m of the section at field site 3 and the surrounding area. The breccia blocks range in size from 0.01 to 2 m, and are composed of partially lithified sandstones and mudstones with bleached white halos surrounding the blocks. The angular blocks occasionally preserve bedding and have downward displaced bedding offsets of < 2 m relative to the surrounding host rock. In the pipes, abundances of breccia blocks range from $\sim 10\%$ to $\sim 90\%$. Breccia pipes are one of the larger pipe types with typical maximum diameters on the order of 1.5–2.5+ m.

Many published studies document breccia pipes and/or breccia blocks in pipes. However, two major types of breccia pipes documented in the Colorado Plateau should be noted here. (1) The first group of breccia pipes includes Jurassic examples such as those in Kodachrome basin (Hannum 1980; Ross et al. 2014), the Laguna region (San Juan Basin) of New Mexico (Schlee 1963; Hunter et al. 1992), and this study, and are interpreted to form through liquefaction and fluidization. These studies document both standard pipes and breccia pipes in their respective study sites along with other pipe expressions. These sites have multiple pipe types such as standard, breccia, and ring-fault pipes, and abundant associated SSD such as tabular dikes (Hannum 1980; Ross et al. 2014) and synsedimentary faults and folds. This group of breccia pipes generally has

TABLE 2.—*Pipe classification scheme and major characteristics.*

Pipe Type	Group	Relief	Coloration	Coloration Relative to Host Rock	Breccia Blocks	Preservation of Original Layering	Grain Sorting	Vertical Extent	Common Stratigraphic Position	Associated Faulting	Avg./Max Grain Size (cm)	Common Diameter (cm)
Standard	1	Positive	White	Different	Very rare	None	Yes	Multiple beds (10+ m)	Common throughout	Occasional	0.05/2–20	10–200
Breccia	1	Cross-section view	Multiple (white matrix)	Same	Many	None (slight with breccia blocks)	None	Multiple beds (0–10 m)	Upper ~ 7 m of section	Occasional	0.05/200	200+
Ring Fault	1	Cross-section view	Multiple	Same	None	Yes	None	Multiple beds (10+ m)	Upper ~ 7 m of section	Yes	0.05/0.05	200+
Rinded Ghost	1	None	Red and white	Same (red) and different (white)	None	None	Yes	Multiple beds (< 10 m)	S_m	None	0.05/0.4	< 65
Combination	1	Varied	Varied	Different	Yes to very rare	None	Sometimes	Multiple beds (< 10 m)	S_m	None	0.05/0.4	< 65
Banded	2	Positive and negative	Multiple (related to host rock)	Different	None	None	None	Multiple beds (changes vertically)	None	None	0.05/0.05	< 65
Mottled	2	None	Red and white	Same (red) and different (white)	None	None	None	Single bed	S_m in lower ~ 5 m of section	None	0.05/0.05	< 65
Coloration	2	None to negative	Dark red/Maroon	Different (Darker)	None	None	None	Single bed	Light pink XB sandstone	None	0.05/0.05	< 65
Ghost	2	None	Red	Same	None	None	None	Single bed	S_m	None	0.05/0.05	< 65
Negative Relief	2	Negative	N/A or red	Different	None	Yes (interior)	None	Single bed	None	None	N/A	< 65

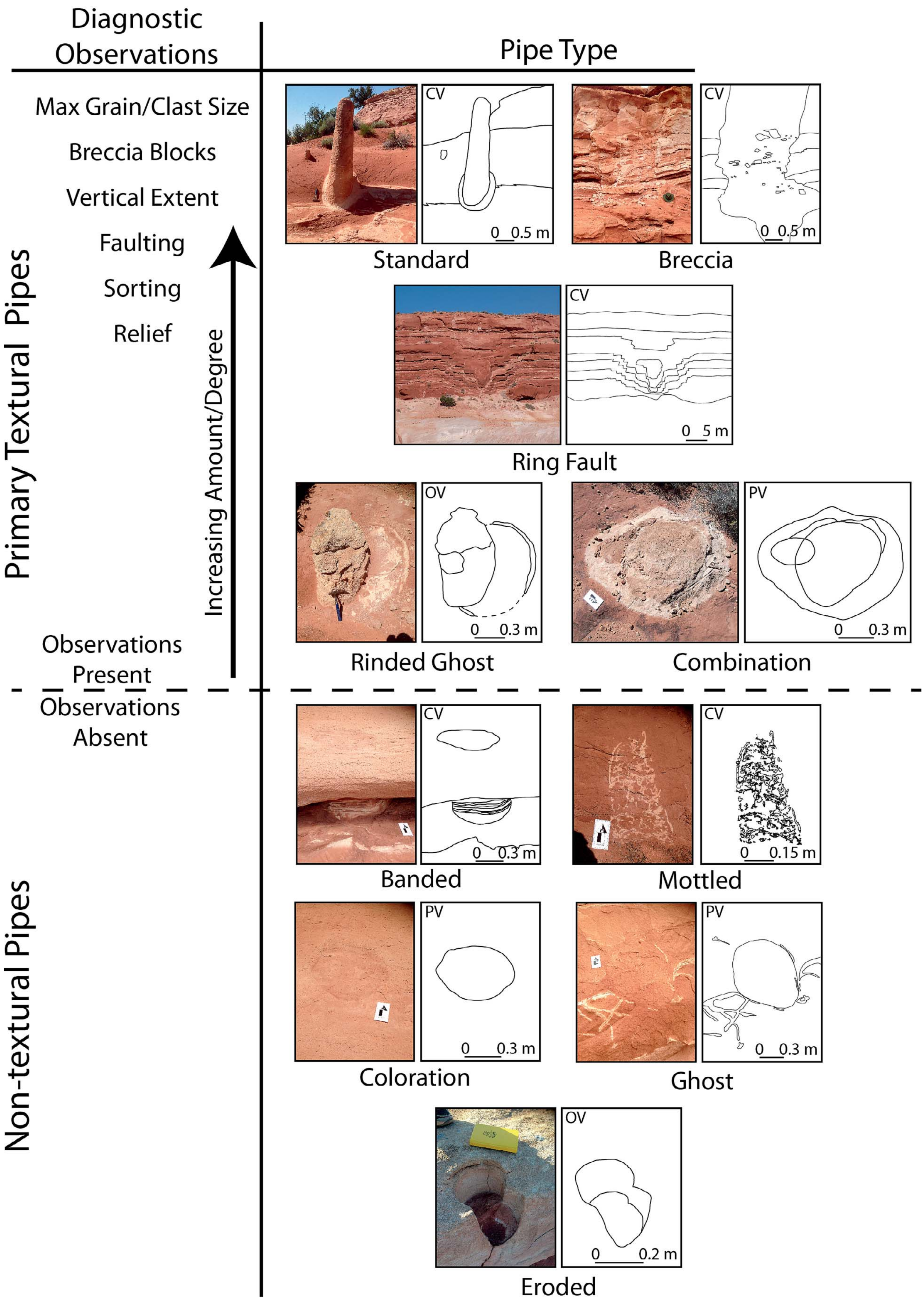
Diagnostic Observations
Pipe Type
Max Grain/Clast Size
Breccia Blocks
Vertical Extent
Faulting
Sorting
Relief
Increasing Amount/Degree
Observations Present
Observations Absent
Primary Textural Pipes
Non-textural Pipes
CV
0 0.5 m
Standard
CV
0 0.5 m
Breccia
CV
0 5 m
Ring Fault
OV
0 0.3 m
Rinded Ghost
PV
0 0.3 m
Combination
CV
0 0.3 m
Banded
CV
0 0.15 m
Mottled
PV
0 0.3 m
Coloration
PV
0 0.3 m
Ghost
OV
0 0.2 m
Eroded

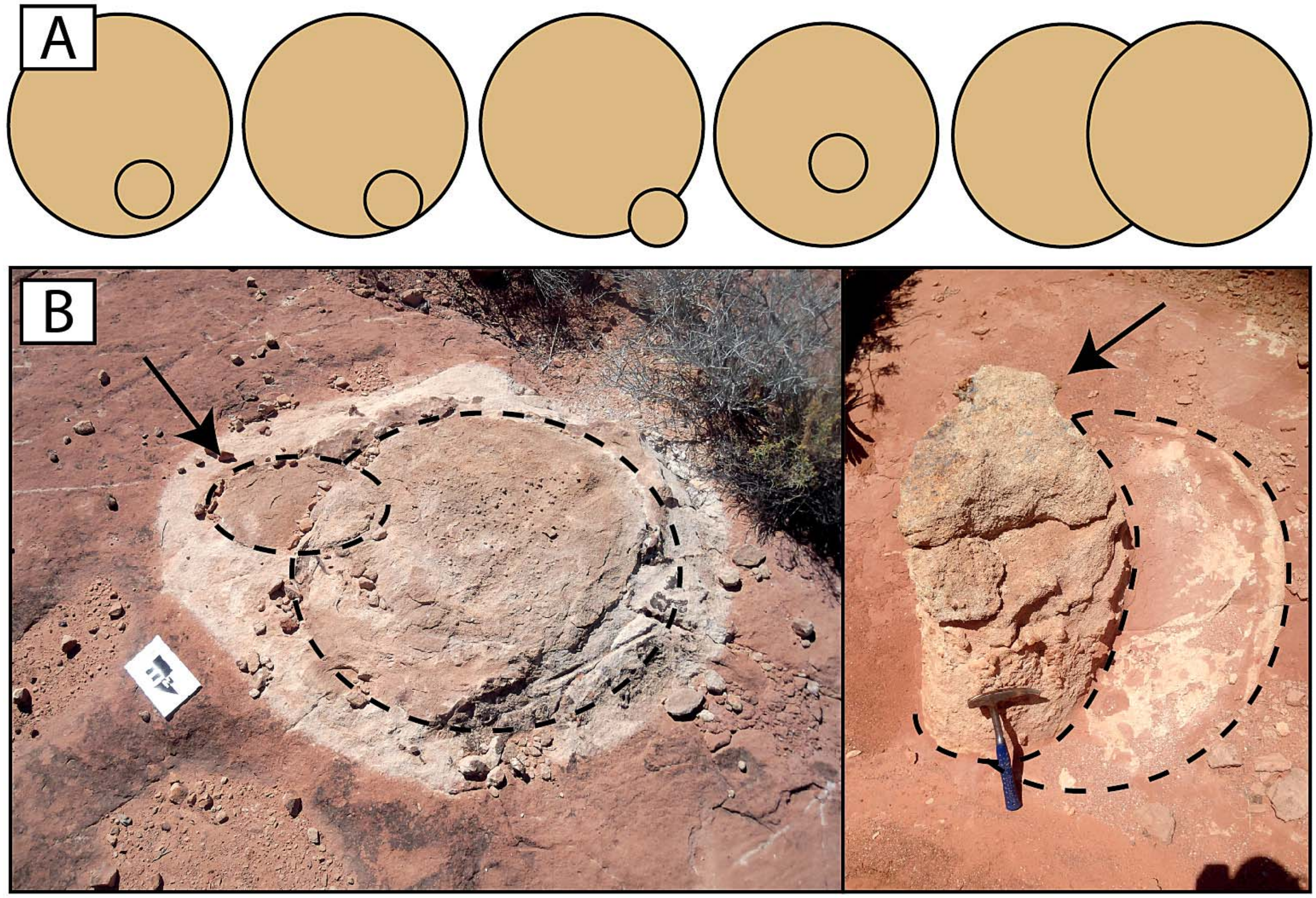

FIG. 12.—**A)** Pipes have several dominant crosscutting geometries with up to five crosscutting pipes (usually two crosscutting pipes). The smaller crosscutting pipe commonly occurs near the outside of the pipe, where the porosity and permeability are highest. **B)** Outcrop images show examples of crosscutting pipes (denoted by the black dashed lines and black arrows).

diameters less than 20 m. (2) A second group of breccia pipes occur without any other associated pipe types or SSD (Wenrich 1985; Wenrich and Huntoon 1989) and have been interpreted to form through limestone dissolution (breccia pipes can also form from the dissolution of gypsum or evaporates; Hunter et al. 1992). These features are commonly associated with karst features and have much larger diameters than the first group of breccia pipes, with diameters up to hundreds of meters (Barrington and Kerr 1963; Weir et al. 1994). The breccia pipes in this study are interpreted to belong to the first group (i.e., formed via fluidization) because of abundant associated SSD, the presence of other pipe types, and the lack of significant beds of limestone, gypsum, and/or evaporates in the surrounding Carmel Formation stratigraphy.

Ring-Fault Pipe.—Ring-fault pipes are internally composed of down-dropped strata that show offset bedding in the host rock (Fig. 11). The pipes have a major, circular ring fault manifest as two vertical faults in cross section (flanking either side of the pipe with symmetrical offsets and spacing). The internal pipe stratification can have offsets up to several meters relative to the host rock. Although some pipes only have the two symmetric bounding faults in cross section (single ring fault), many others have multiple sets of synsedimentary faults moving away from the pipe. The series of faults with successive downward offsets towards the pipe give them a stair-stepped appearance. These faults likely represent multiple concentric ring faults. Some ring-fault pipes have a standard pipe at the center of the concentric faults. However, some views show only the concentric, circular ring faults and down-dropped strata. Ring-fault pipes occur most commonly in the upper 7 m of the pipe-bearing section, and almost exclusively viewed in vertical cross section. These pipes are similar to the ones described by Hunter et al. (1992) in the San Juan Basin of New Mexico and Netoff (2002) in the Lake Powell region. Netoff (2002) observes some ring faults in a horizontal map view confirming the ring geometry surrounding the pipe.

Combination Pipe.—Combination pipes are defined as two crosscutting pipes of either the same type or different types (Deynoux et al. 1990). The crosscutting pipe is typically smaller and occurs on the outer part of the larger pipe (Figs. 11, 12). Combination pipes most commonly occur in sets of two; however, they can occur with up to five crosscutting pipes. The

←

FIG. 11.—Pipes are classified into two groups: 1) primary textural pipes (orange in Table 2), and 2) non-textural pipes (blue in Table 2). Primary textural pipes have grain sorting, a maximum grain size larger than the surrounding host rock, breccia blocks, positive relief, and associated host-rock synsedimentary faulting. They maintain these characteristics vertically across boundaries between stratigraphic layers. Non-textural pipes do not have any textural differences from the host rock.

most common arrangements include two standard pipes and a standard pipe crosscutting a rinded ghost pipe (discussed below).

Non-Textural Pipes

Ghost Pipe.—Ghost pipes are circular features with no positive relief and a color similar to that of the host rock (Fig. 11). Ghost pipes have two internal expressions: one with a rind and one without. When a ghost pipe has a rind, the rind is composed of bleached white, fine- to coarse-grained sandstone with abundant volcanic fragments ranging up to pebble size. These pipes are stratigraphically restricted to a single bed (i.e., they do not cross layer boundaries) and commonly occur in the S_m, S_{mc}, and S_{rc} facies.

Coloration Pipe.—Coloration pipes are stratigraphically constrained to a single ~ 1.5–3 m bed and are most common at field site 3. They have a darker maroon coloration (10R 5/4) relative to the light pink or red (10R 6/3 or 6/4) host rock, and have either a slight depression from weathering or no relief (Fig. 11). Other than coloration and slight relief differences, coloration pipes display few textural differences from the host rock. They are composed of medium-grained sandstone similar in size and composition to the surrounding rock, and have no internal sorting. Coloration pipes occur most commonly in the S_m, S_{cb}, and S_{dc} facies

Mottled Pipe.—Mottled pipes are cylindrical expressions of irregularly bleached sandstone (Fig. 11). The irregular bleached shapes cluster within a larger cylindrical shape, and have the same composition and grain size as the host rock in addition to no internal sorting. These pipes are directly associated with zones of diagenetic bleaching and irregular sandstone bodies (S_{ib}). The most prevalent zone of mottled pipes occurs low in the pipe-bearing section at field site 3, particularly in the S_m facies.

Eroded Pipe.—Eroded pipes are rare and constitute < 1% of observed pipes. As their name implies, they have negative relief and are cylindrical negatives in the host rock (Fig. 11). They range in size from tens of centimeters to meters in diameter. At the base they are typically composed of red (10R 5/8 or 4/6) sandstone.

Banded Pipe.—Banded pipes are some of the most unusual, yet most useful, examples for interpreting pipe formation processes. Banded pipes change character as they pass through different stratigraphic layers. Although still vertically oriented and cylindrical, banded pipes have internal horizontal stratification. The internal stratigraphic banding corresponds to the bedding in the surrounding host rock. Internally, each stratified pipe band resembles a non-textural pipe type such as a coloration pipe. Many non-textural pipes are stratigraphically restricted to a single bed or layer when observed individually. However, several critical exposures reveal that non-textural pipes can form a vertical succession of bands comprising a single feature (Fig. 11). As the pipe crosscuts the stratigraphic column it changes pipe types at each layer. This indicates that pipes respond to different lithologies and have different expressions controlled chiefly by host-rock characteristics.

DISCUSSION

The Pipe System

The pipe-system model has a porous coarse-grained source, an impermeable overlying fine-grained pressurizing layer, a succession of host sediments, and an eruption surface (Obermeier 1996). All four pipe-system elements are present in the Carmel Formation study section. The pipe system is stratigraphically bounded with pipes occurring almost exclusively in the Paria River Member of the Carmel Formation (Fig. 4).

The pipes originated from an ~ 1–2 m-thick fluvial sandstone source in the underlying Crystal Creek Member and moved upwards through an ~ 1-m-thick pressurizing mudstone layer (Fig. 13). The fluvial source bed is the only reasonable coarse-grained layer that could have sourced the pipes, due to its stratigraphic position. Examples of pipes moving from the source bed through the confining layer into the host rock (Fig. 13), and its extensive associated SSD (contorted and undulating bedding), further support this conclusion. The source bed is composed of fine- to coarse-grained quartz sandstone with granule to pebble-size volcanic fragments. The fluvial source contains numerous (> 50% by volume in some places) mudstone clasts, interpreted to be ripped up from the overlying confining layer during pipe emplacement. Although the source bed varies in thickness throughout the outcrop bench and is absent in places, the mudstone pressurizing layer remains a relatively continuous thickness across the ~ 8 km of cliff-face outcrop exposure between the field sites. The pipes terminate at the uppermost bed of the Paria River Member, with some exhibiting outward flaring geometries (Figs. 4, 5), implying that they erupted onto a paleosurface (Netoff 2002; Livingston et al. 2014; Sherrod et al. 2016). Pipes that exhibit flaring occur only in several correlative horizons (Fig. 4), suggesting multiple eruption surfaces.

Formation Mechanism

These Jurassic Carmel Formation pipes and their associated SSD features form due to liquefaction and fluidization. These separate but related processes occur as a result of reduced sediment strength due to interactions with pore fluids, and cause sediment to behave like a liquid (Owen 1987). Liquefaction occurs when increased pore pressure equals the overburden pressure, while fluidization results when the frictional (i.e., drag) forces of a fluid moving through the system equal the downward-acting forces on the sediment (Owen 1987; Obermeier 1996; Owen and Moretti 2011; Ross et al. 2014). During pipe formation, liquefaction is triggered by strong ground motion and creates overpressure in the system. This results in the formation of contorted bedding. Fluidization occurs as the pressurizing layer fails due to hydrofracture and transports sediment in a sediment–water slurry, resulting in pipe formation. Owen (1987), Obermeier (1996), and Ross et al (2011, 2014) provide excellent summaries of the theory and equations that govern liquefaction and fluidization as well as the features that these processes create.

In the field area, pipes flare outwards at 2 or 3 correlative horizons (eruption horizons) separated by several meters of sedimentation, and have crosscutting relationships with up to five crosscutting pipes. This evidence points to multiple, discrete pipe-forming events. Brecciation, grain sorting, traction structures (such as the outer rind), and a cylindrical geometry all indicate a violent formation mechanism that involved suspended-sediment transport in a fluid medium. A fluvial sandstone bed at the base of the pipe-bearing section contains SSD, pieces of entrained mudstone clasts from the confining layer, and several examples of pipes moving up from the bed through the overlying mudstone and into the host rock. This demonstrates an upward movement of material into and through the host rock. Finally, concentric ring faults, with successive downward offsets in towards the pipes, indicate relaxation structures likely the result of reduction of sediment volume when grain contacts are reestablished during dewatering. In one case, the down-dropped blocks show rotation towards the pipe, indicating sediment collapse (Fig. 10). These lines of evidence collectively illustrate that the pipes formed as a result of multiple fluidization events: (1) multiple eruption horizons, (2) crosscutting pipes, (3) a violent formation mechanism, (4) transport in a fluid medium, (5) upwards movement of material, and (6) dewatering structures. The fluidization events could have been triggered by earthquakes. Although extremely large earthquakes at the Cordilleran margin could have triggered pipe formation at this study site, reactivation of deep basement structures, particularly the Kaibab monocline 10 km to the west, is a more likely source for the strong

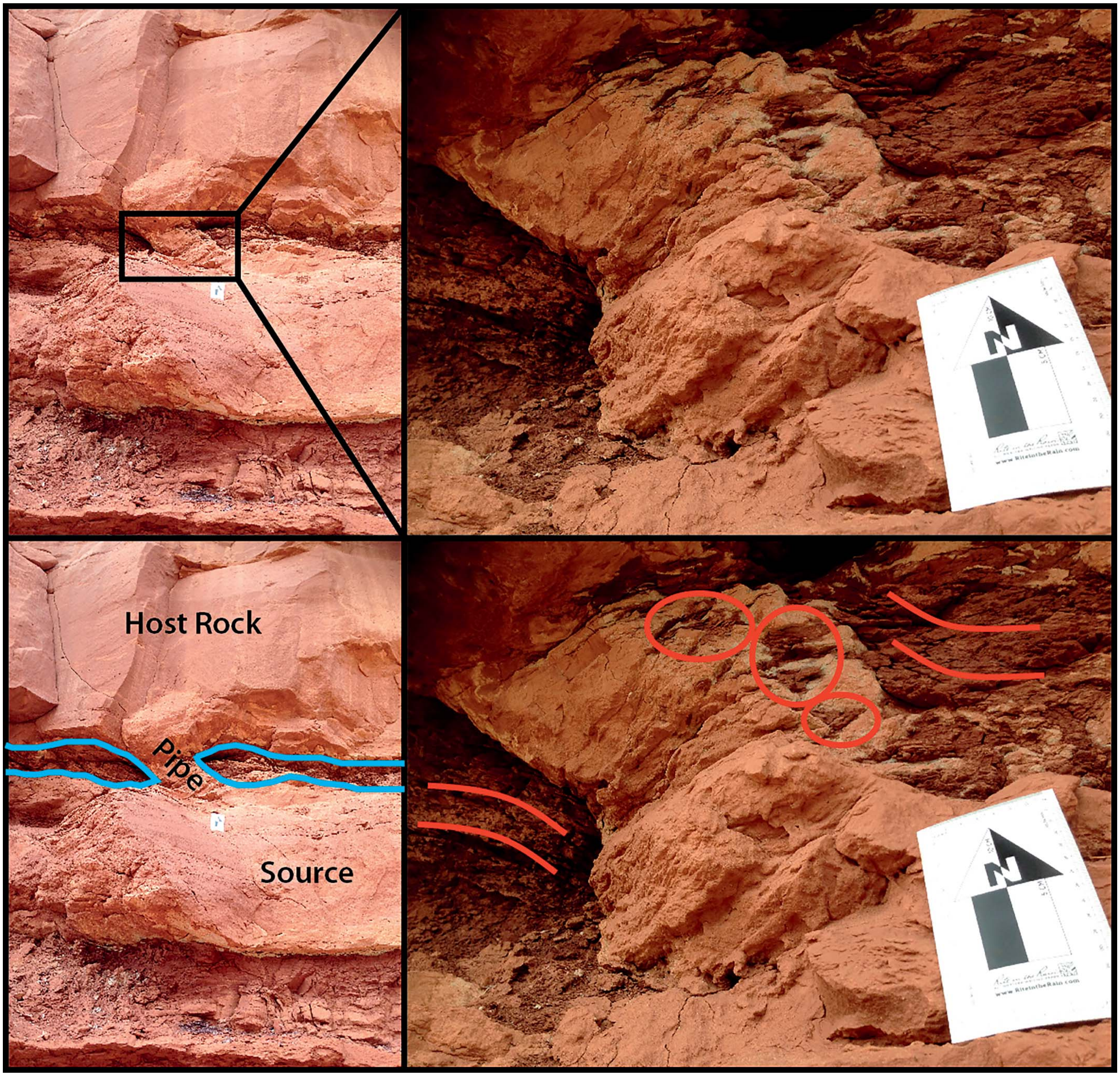

FIG. 13.—Several pipes emanate from the source bed, move through the seal (mudstone), and crosscut the host rock (out of plane in this example). Mudstone laminae lip upwards and downwards as they meet the pipe, and broken pieces of mudstone are incorporated into the pipe. These mudstone clasts have bleached halos from reducing diagenetic fluids.

ground motion necessary to trigger pipe formation (Wheatley et al. 2016). Obermeier (1996) uses modern and historical data to demonstrate that an earthquake with a moment magnitude of 5–6 can generate liquefaction and fluidization features up to 10 km from the epicenter, and an earthquake with a moment magnitude of 8+ can generate liquefaction and/or fluidization features over 200 km from the epicenter (the approximate distance to the Cordilleran margin).

Pipe formation occurs in a five-step sequence. (1) Porous, water-saturated sands present beneath a fine-grained sealing layer create ideal conditions for pipe formation. In addition to this facies arrangement, which creates the necessary conditions for fluidization, the host rock plays a key role in determining the resulting geometry of the injectite. Cylindrical injectites (i.e., pipes) preferentially form in relatively isotropic sandstone host rock, in contrast to tabular geometries (i.e., dikes), which tend to form in more anisotropic mudstones. (2) The forceful upward injection of clastic material via fluidization due to overpressurization induced by strong ground motion causes fluids to brecciate the host rock, entraining sandstone and mudstone pieces of the host rock in the pipes. The process of material injection and fluidization deforms the host rock, causing the synsedimentary formation of folds and faults in the host rock. Some pipes

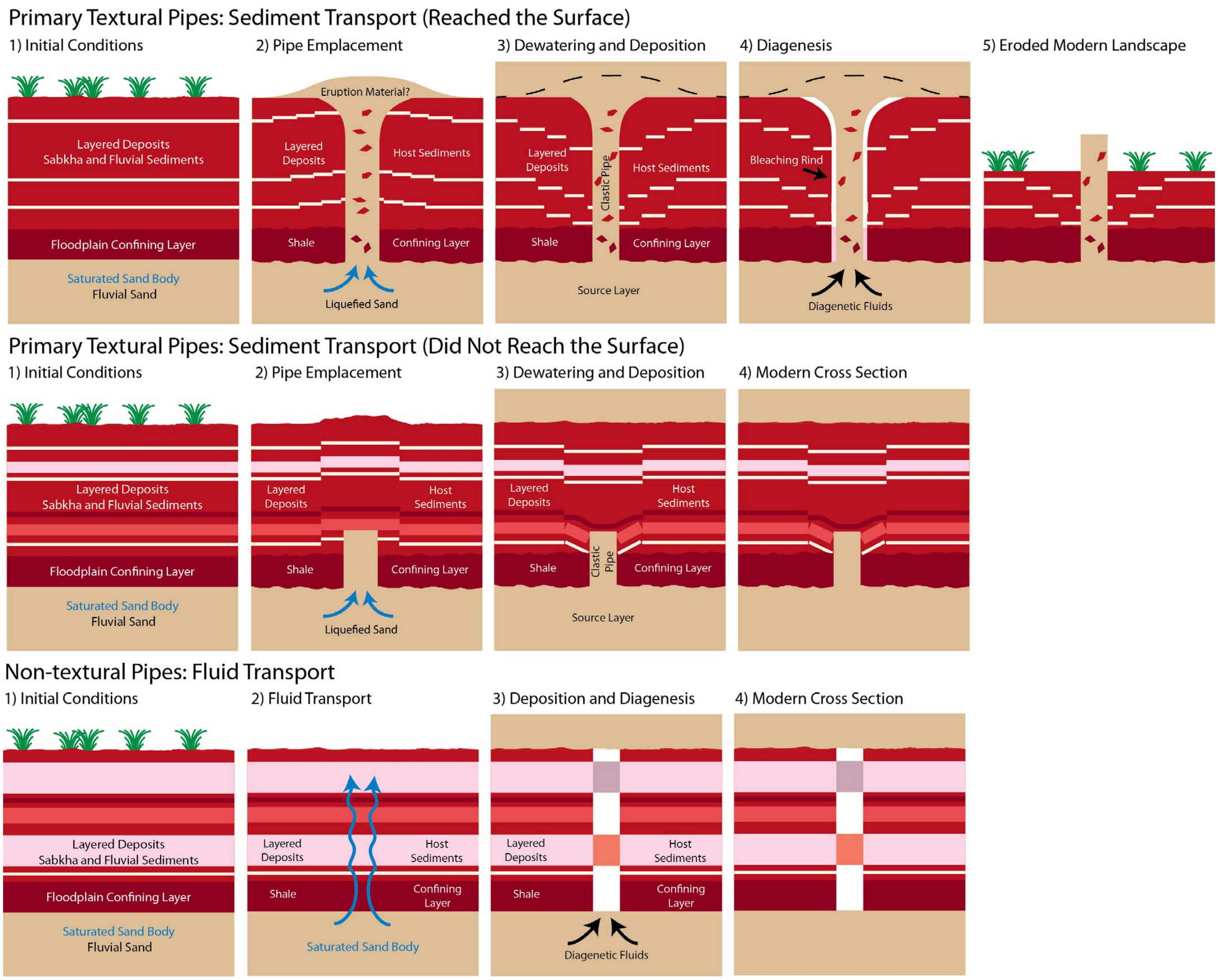

FIG. 14.—Primary textural pipes form by the upwards movement of fluidized sediment. These pipes can either reach the surface as sand volcanoes with flaring geometries, or do not reach the surface with host-rock layers continuing across the top of the pipes. Non-textural pipes form through upwards fluid movement. These fluids winnow out any fine-grained sediments to form preferential fluid pathways but are too weak to fully fluidize the sediment. These pipes have diagenetic differences relative to the host rock that can change at bedding boundaries (modified from Wheatley et al. 2016).

reach the surface as sand volcanoes creating an eruption surface, which is preserved as the outward-flaring geometries present in pipes (Livingston et al. 2014). Other pipes likely do not reach the surface, given observed terminations and relationships with the host rock. (3) After pipe emplacement, pipes undergo a dewatering phase which results in sediment volume reduction and the formation of collapse structures (e.g., ring faults) as the water pressure dissipates. Subsequent to dewatering, normal depositional processes resume, reworking the surface eruption sediments. (4) Pipes then act as fluid conduits for later diagenetic fluids which cement and bleach the pipes. (5) Finally, the more indurated and preferentially cemented pipes weather out in positive relief in the washes and cliffs of the modern landscape (Fig. 14). This process, interpreted from field observations, has been replicated in the laboratory via physical modeling, including the downward movement of breccia blocks in the upwards-moving column of sand (Nichols et al. 1994; Frey et al. 2009; Rodrigues et al. 2009; Ross et al. 2011).

Controls on Pipe Expressions

Pipes have a variety of physical expressions, each with a diagnostic set of observable characteristics (Fig. 11). These physical expressions can be linked to various processes and provide a more complete picture of pipe formation. The various pipe types can be separated into two major groups, each with a related but different interpreted formation mechanism: (1) dominantly sediment transport (i.e., injection) features termed *primary textural pipes* (standard, breccia, ring-fault, rinded-ghost, and combination pipes), and (2) dominantly fluid transport features termed *non-textural pipes* (coloration, ghost, mottled, and banded pipes) (Fig. 11). Primary textural pipes have sediment sorting, indicating movement of sediment suspended in a fluid. In addition, the textural pipes have a maximum grain size or clast size larger than the surrounding host rock, breccia blocks, associated faulting in the host rock, and/or positive relief from weathering. These pipe types crosscut multiple beds and maintain their characteristics throughout the vertical length of the pipe. Non-textural pipes lack these characteristics and instead occur in only a single stratigraphic zone and/or

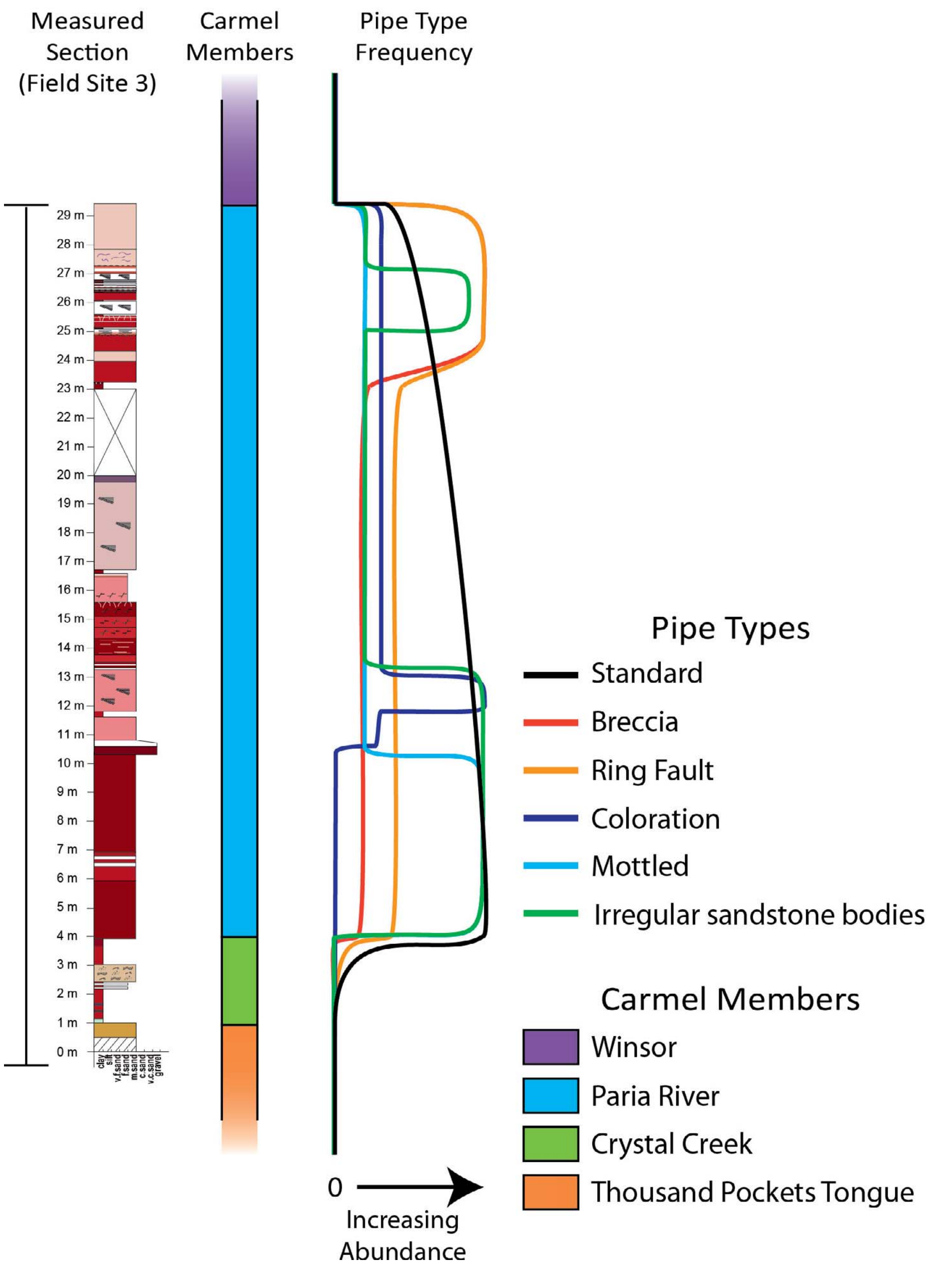

FIG. 15.—Different pipe types occur in different abundances stratigraphically. Standard pipes occur throughout the section but decrease in frequency up section. Breccia and ring-fault pipes occur in the upper ~ 7 m of the section. Coloration pipes, mottled pipes, and irregular sandstone bodies occur at several distinct beds in the section.

host-rock facies. Host-rock properties are the dominant control on non-textural pipe expressions.

Primary Textural Pipes.—Primary textural pipes are interpreted to form through fluidization of the sediment (Fig. 14). The grain sorting present in standard pipes and the brecciation in breccia pipes point to a violent injection event with moving sediment suspended in a fluid medium. In the primary textural pipe grouping, ring-fault pipes possess many of the group characteristics; however, the preservation of host-rock bedding in the pipe suggests that ring-fault pipes represent an expression related to sediment injection. They most likely represent either: (1) a cross-sectional view of ring faults, which commonly surround pipes (i.e., the cross-sectional cut did not intersect the pipe), or (2) the region above a pipe that did not reach the surface. Several pipes have stratigraphic relationships which indicate that they did not reach the surface. However, some synsedimentary faulting continues vertically beyond the pipe to what has been interpreted as a paleo-surface based on pipe flaring geometries (Fig. 10C). The stratigraphy above the pipe that is bounded by the ring fault is offset downwards and has the expression identical to a ring-fault pipe (Figs. 10, 11). This interpretation would also explain why the majority of ring-fault pipes occur in the uppermost part of the section.

Non-Textural Pipes.—Non-textural pipes are also related to liquefaction and fluidization, but they formed through a slightly different process. These pipes form as synsedimentary features, which are then visually enhanced by subsequent diagenetic fluids. Sediment fluidizes when the upward forces (drag) caused by water moving through the sediment exceed the downward forces (gravitational body force) (Owen 1987; Obermeier 1996; Ross et al. 2011). In the pipe system there could be regions and events where the upward-moving fluids did not have sufficient energy to fluidize the sand (e.g., fluids moving through previously created fractures in the sealing layer from an earlier pipe forming event). However, the upward-moving fluids would have been able to winnow out the clay and silt common in the sands of the Carmel Formation. As fluids move upward through the host rock they winnow out the fine-grained sediment, creating fluid conduits for later diagenetic fluids. This process occurs without any physical sorting of the sand or brecciation of the host rock (Fig. 14). This process would explain why the pipe expressions are restricted to a single layer, have the same grain size and textural characteristics as the host rock, and have no grain sorting or brecciation. Host-rock properties are the dominant controls on non-textural pipe expressions. Banded pipes demonstrate this host-rock control. They display a vertical series of pipe expressions that change at the interface between different beds.

CONCLUSIONS

The Carmel Formation in southern Utah is the ideal place to understand ancient pipe-forming mechanisms and controls. The sedimentological context (i.e., facies associations) indicate that pipes formed preferentially in the wetter sabkha and fluvial strata of the Middle Jurassic arid continental system. The pipes are located near several basement structures where multiple reactivation events likely triggered multiple pipe-forming events. These liquefaction and fluidization events resulted in significant disruption of original bedding and the formation of synsedimentary faults and folds, in addition to thousands of pipes. The dominance of pipes in sandstone deposits (with a distinct lack of mudstone intervals and dike-injection geometries) suggests that pipes are the preferred injectite geometry for sand systems which are more isotropic than their fine-grained counterparts.

The pipe types in the study area are separated into two groups: (1) primary textural pipes, with five distinct variants or types formed by liquefaction and fluidization, and (2) non-textural pipes, with five distinct variants or types formed by weaker upwards fluid movement that was unable to fully fluidize the sand-size sediment. Primary textural pipes have grain sorting, a maximum grain or clast size greater than the surrounding host rock, brecciation of the host rock, positive relief, and/or associated host-rock synsedimentary faulting. These pipes crosscut multiple host-rock beds and maintain their characteristics throughout the vertical extent of the pipe. Non-textural pipes lack these characteristics, and they are stratigraphically constrained to a single bed. The dominant control on the expression of non-textural pipes is the host-rock properties. The variability of host-rock sandstone appearance in the Carmel Formation, largely a result of diagenesis, clearly illustrates this control, with many non-textural pipes corresponding to specific intervals in the section (Fig 15).

These pipes follow a larger facies-controlled trend in Utah that forms an arcuate band from this study area to Moab paralleling the paleoshoreline of the Sundance Sea (Wheatley et al. 2016). The pipes form preferentially in sabkha sediments because of (1) the high water table (i.e., water saturation), (2) the interfingering of fine- and coarse-grained facies (i.e., a source overlain by a seal), and (3) the loosely packed nature of the sediments, i.e., highly susceptible to liquefaction or fluidization. These three factors make the sabkha sediments rimming the Sundance Sea the ideal pipe-forming environment. Pipes can show a wide range of geometries, sizes, and expressions. In the context of their stratigraphic positions pipes can be valuable indicators of paleoenvironmental conditions (e.g., high water table), tectonic triggers, and preferential fluid flow pathways in sandstone lithologies.

SUPPLEMENTAL MATERIAL

The Pipe Characteristic Database is available from JSR's data archive: https://www.sepm.org/pages.aspx?pageid=229.

ACKNOWLEDGMENTS

We appreciate the constructive reviews of Gary Weissmann, Sally Potter-McIntyre, and Gary Nichols. A special thank you to Mark Hansford and Ian Treat for their invaluable help with field work, insightful discussions, and initial reads of the manuscript. We acknowledge Kellan Warner, Katy Foltz, and Steve Tillman for their field assistance, and Douglas Sprinkel, Hobie Willis, and Christian Hardwick at the Utah Geological Survey for their field input and help with processing the GPS data. We are grateful to Jeff Fry, Kevin Miller, and the staff at the Grand Staircase–Escalante National Monument and Paria Outpost Station for their logistical support. Irv Kranzler brought the field site to our attention and gave continuous encouragement throughout the project. The GDL Foundation (Structural Diagenesis Fellowship), the Rocky Mountain Association of Geologists (Norman H. Foster Memorial Scholarship), the National Aeronautics and Space Administration (NASA-EPOESS grant NNX11AH29G), the Geological Society of America (Grants-in-Aid Program), the American Association of Petroleum Geologists (Allan and Eleanor Martini Grant), and the Wheaton College Scholastic Honor Society provided financial support.

REFERENCES

Alvarez, W., Staley, E., O'Connor, D., and Chan, M., 1998, Synsedimentary deformation in the Jurassic of southeastern Utah: a case of impact shaking? Geology, v. 26, p. 579–582.

Baer, J.L., and Steed, R.H., 2010, Geology of Kodachrome Basin State Park, Utah: Utah Geological Association, Publication 28, p. 467–482.

Barrington, J., and Kerr, P., 1963, Collapse features and silica plugs near Cameron, Arizona: Geological Society of America, Bulletin 74, p. 1237–1258.

Blakey, R.C., 1994, Paleogeographic and tectonic controls on some Lower and Middle Jurassic erg deposits, Colorado Plateau, *in* Reynolds, M.W., and Dolly, E.D., eds., Mesozoic Systems of the Rocky Mountain Region, USA: SEPM, Rocky Mountain Section, p. 273–298.

Blakey, R.C., Peterson, F., Caputo, M.V., Geesaman, R.C., and Voorhees, B.J., 1983, Paleogeography of Middle Jurassic continental, shoreline, and shallow marine sedimentation, southern Utah, *in* Caputo, M.V., Peterson, J.A., and Franczyk, K.J., eds., Mesozoic Paleogeography of West Central United States: SEPM, Rocky Mountain Section, p. 77–100.

Chan, M., Kocurek, G., Netoff, D., Alvarez, W., and Blakey, R., 2007, Clastic-injection pipes and syndepositional deformation structures in Jurassic eolian deposits: examples from the Colorado Plateau, *in* Hurst A., and Cartwright, J., eds., Sand Injectites: Implications for Hydrocarbon Exploration and Production: American Association of Petroleum Geologists, Memoir 87, p. 233–244. https://doi.org/10.1306/1209867M871350

Chapman, M., 1987, Depositional and compositional aspects of volcanogenic clasts in the Upper Member of the Carmel Formation, southern Utah [MS Thesis]: Northern Arizona University, p. 93 p. https://doi.org/10.1017/CBO9781107415324.004

Chapman, M.G., 1989, Implications of rhyolitic ignimbrite boulders in the Middle Jurassic Carmel Formation of southern Utah: Geology, v. 17, p. 281–284.

Chapman, M.G., 1993, Catastrophic floods during the Middle Jurassic: evidence in the Upper Member and Crystal Creek Member of the Carmel Formation, southern Utah: SEPM, Pacific Section, p. 407–416.

Deynoux, M., Proust, J.N., Durand, J., and Merino, E., 1990, Water-transfer cylindrical structures in the late Proterozoic eolian sandstones in the Taoudeni Basin West Africa: Sedimentary Geology, v. 66, p. 227–242.

Dickinson, W.R., Stair, K.N., Gehrels, G.E., Peters, L., Kowallis, B.J., Blakey, R.C., Amar, J.R., and Greenhalgh, B.W., 2010, U-Pb and $^{40}Ar/^{39}Ar$ ages for a tephra lens in the Middle Jurassic Page Sandstone: first direct isotopic dating of a Mesozoic eolianite on the Colorado Plateau: The Journal of Geology, v. 118, p. 215–221. https://doi.org/10.1086/649819

Doelling, H.H., and Willis, G.C., 2006, Geologic map of the Smokey Mountain $30' \times 60'$ Quadrangle, Kane and San Juan Counties, Utah, and Coconino County, Arizona: Utah Geological Survey, Map 213, 2 Plates, Scale 1:100,000.

Doelling, H.H., Sprinkel, D.A., Kowallis, B.J., and Kuehne, P.A., 2013, Temple Cap and Carmel Formations in the Henry Mountains Basin, Wayne and Garfield Counties, Utah: Utah Geological Association, Publication 42, p. 279–318.

Draganits, E., Grasemann, B., and Schmid, H.P., 2003, Fluidization pipes and spring pits in a Gondwanan barrier-island environment: groundwater phenomenon, palaeo-seismicity or a combination of both?, *in* Vanrensbergen, P., Hillis, R.R., Maltman, A.J., and Morley, C.K., eds., Subsurface Sediment Mobilization: Geological Society of London, Special Publication 216, p. 109–121.

Dubiel, R., Huntoon, J., Stanesco, J., and Hasiotis, S., 2014, Depositional setting of the Hoskinnini Member of the Triassic Moenkopi Formation, southeastern Utah: Utah Geological Association, Publication 43, p. 296–310.

Duranti, D., and Hurst, A., 2004, Fluidization and injection in the deep-water sandstones of the Eocene Alba Formation (UK North Sea): Sedimentology, v. 51, p. 503–529. https://doi.org/10.1111/j.1365-3091.2004.00634.x

Frey, S.E., Gingras, M.K., and Dashtgard, S.E., 2009, Experimental studies of gas-escape and water-escape structures: mechanisms and morphologies: Journal of Sedimentary Research, v. 79, p. 808–816. https://doi.org/10.2110/jsr.2009.087

FREY-MARTINEZ, J., HALL, B., CARTWRIGHT, J., AND HUUSE, M., 2007, Clastic intrusion at the base of deep-water sands: a trap-forming mechanism in the eastern Mediterranean, *in* Hurst, A., and Cartwright, J., eds., Sand Injectites: Implications for Hydrocarbon Exploration and Production: American Association of Petroleum Geologists, Memoir 87, p. 49–63.

GUHMAN, A.I., AND PEDERSON, D.T., 1992, Boiling sand springs, Dismal River, Nebraska: agents for formation of vertical cylindrical structures and geomorphic change: Geology, v. 20, p. 8–10. https://doi.org/10.1130/0091-7613(1992)020<0008

HANNUM, C., 1980, Sandstone and conglomerate–breccia pipes and dikes of the Kodachrome Basin area, Kane County, Utah [MS Thesis]: Brigham Young University, p. 1–50.

HUBBARD, S.M., ROMANS, B.W., AND GRAHAM, S.A., 2007, An outcrop example of large-scale conglomeratic intrusions sourced from deep-water channel deposits, Cerro Toro Formation, Magallanes Basin, Southern Chile, *in* Hurst A., and Cartwright, J., eds., Sand Injectites: Implications for Hydrocarbon Exploration and Production: American Association of Petroleum Geologists, Memoir 87, p. 199–207. https://doi.org/10.1306/1209863M873265

HUNTER, R.E., GELFENBAUM, G., AND RUBIN, D.M., 1992, Clastic pipes of probable solution-collapse origin in Jurassic rocks of the southern San Juan Basin, New Mexico: U.S. Geological Survey, Bulletin 1808, p. 1–19.

HURST, A., SCOTT, A., AND VIGORITO, M., 2011, Physical characteristics of sand injectites: Earth-Science Reviews, v. 106, p. 215–246. https://doi.org/10.1016/j.earscirev.2011.02.004

HUUSE, M., AND MICKELSON, M., 2004, Eocene sandstone intrusions in the Tampen Spur area (Norwegian North Sea quad 34) imaged by 3D seismic data: Marine and Petroleum Geology, v. 21, p. 141–155. https://doi.org/10.1016/j.marpetgeo.2003.11.018

JONES, L.S., AND BLAKEY, R.C., 1997, Eolian–fluvial interaction in the Page Sandstone (Middle Jurassic) in south-central Utah, USA: a case study of erg-margin processes: Sedimentary Geology, v. 109, p. 181–198. https://doi.org/10.1016/S0037-0738(96)00044-9

KOWALLIS, B.J., CHRISTIANSEN, E.H., DEINO, A.L., ZHANG, C., AND EVERETT, B.H., 2001, The record of Middle Jurassic volcanism in the Carmel and Temple Cap formations of southwestern Utah: Geological Society of America, Bulletin 113, p. 373–387. https://doi.org/10.1130/0016-7606(2001)113<0373:TROMJV>2.0.CO;2

KOWALLIS, B.J., SPRINKEL, D.A., CHRISTIANSEN, E.H., STEED, S., WHEATLEY, D.F., AND JICHA, B., in prep, Rhyolite ignimbrite boulders and cobbles in the Middle Jurassic Carmel Formation of Utah and Arizona: new data on age, composition, and transport.

LIVINGSTON, K.M., BOGNER, E., IRELAND, S., SIMPSON, E., BETTS, T., AND LAUB, E., 2014, The geomorphic evolution of shallow-sourced methane produced mud volcanoes: Lake Powell, Hite, Utah [Abstract]: Geological Society of America, Abstracts with Programs, no. 320–3.

LOOPE, D.B., ELDER, J.F., ZLOTNIK, V.A., KETTLER, R.M., AND PEDERSON, D.T., 2013, Jurassic earthquake sequence recorded by multiple generations of sand blows, Zion National Park, Utah: Geology, v. 41, p. 1131–1134. https://doi.org/10.1130/G34619.1

MOSS, J.L., AND CARTWRIGHT, J., 2010, 3D Seismic expression of km-scale fluid escape pipes from offshore Namibia: Basin Research, v. 22, p. 481–501. https://doi.org/10.1111/j.1365-2117.2010.00461.x

MUNSELL SOIL COLOR CHARTS, 2000, New Windsor, N.Y.: Munsell Color.

NETOFF, D., 2002, Seismogenically induced fluidization of Jurassic erg sands, south-central Utah: Sedimentology, v. 49, p. 65–80. https://doi.org/10.1046/j.1365-3091.2002.00432.x

NETOFF, D.I., AND SHROBA, R.R., 2001, Conical sandstone landforms cored with clastic pipes in Glen Canyon National Recreation Area, southeastern Utah: Geomorphology, v. 39, p. 99–110. https://doi.org/10.1016/S0169-555X(00)00096-9

NICHOLS, R.J., SPARKS, R.S.J., AND WILSON, C.J.N., 1994, Experimental studies of the fluidization of layered sediments and the formation of fluid escape structures: Sedimentology, v. 41, p. 233–253.

OBERMEIER, S.F., 1996, Using liquefaction-induced features for paleoseismic analysis, *in* McCalpin, J., eds., Paleoseismology: San Diego: Academic Press, p. 331–396.

OWEN, G., 1987, Deformation processes in unconsolidated sands, *in* Jones, M.E., and Preston, R.M.F., eds., Deformation of Sediments and Sedimentary Rocks: Geological Society of London, Special Publication 29, p. 11–24. https://doi.org/10.1144/GSL.SP.1987.029.01.02

OWEN, G., AND MORETTI, M., 2011, Identifying triggers for liquefaction-induced soft-sediment deformation in sands: Sedimentary Geology, v. 235, p. 141–147. https://doi.org/10.1016/j.sedgeo.2010.10.003

PETERSON, F., 1994, Sand dunes, sabkhas, streams, and shallow seas: Jurassic paleogeography in the southern part of the western interior basin, *in* Reynolds, M.W., and Dolly, E.D., eds., Mesozoic Systems of the Rocky Mountain Region, USA: SEPM, Rocky Mountain Section, p. 233–272.

PHOENIX, D., 1958, Sandstone cylinders as possible guides to paleomovement of ground water, *in* Anderson, R.Y., and Harshbarger, J.W., eds., Black Mesa Basin (Northeastern Arizona): New Mexico Geological Society, 9th Annual Fall Field Conference, Guidebook, p. 194–196.

RODRIGUES, N., COBBOLD, P.R., AND LØSETH, H., 2009, Physical modelling of sand injectites: Tectonophysics, v. 474, p. 610–632. https://doi.org/10.1016/j.tecto.2009.04.032

ROSS, J.A., PEAKALL, J., AND KEEVIL, G.M., 2011, An integrated model of extrusive sand injectites in cohesionless sediments: Sedimentology, v. 58, p. 1693–1715. https://doi.org/10.1111/j.1365-3091.2011.01230.x

ROSS, J.A., PEAKALL, J., AND KEEVIL, G.M., 2014, Facies and flow regimes of sandstone-hosted columnar intrusions: insights from the pipes of Kodachrome Basin State Park: Sedimentology, v. 61, p. 1764–1792. https://doi.org/10.1111/sed.12115

SAUCIER, R.T., 1989, Evidence for episodic sand-blow activity during the 1811–1812 New Madrid (Missouri) earthquake series: Geology, v. 17, p. 103–106. https://doi.org/10.1130/0091-7613(1989)017<0103:EFESBA>2.3.CO;2

SCHLEE, J.S., 1963, Sandstone pipes of the Laguna area, New Mexico: Journal of Sedimentary Petrology, v. 33, p. 112–123. https://doi.org/10.1306/74D70DE4-2B21-11D7-8648000102C1865D

SHERROD, L., SIMPSON, E.L., HIGGINS, R., MILLER, K., MORGANO, K., SNYDER, E., AND VALES, D., 2016, Subsurface structure of water–gas escape features revealed by ground-penetrating radar and electrical resistivity tomography, Glen Canyon National Recreation Area, Lake Powell delta, Utah, USA: Sedimentary Geology, v. 344, p. 160–174. https://doi.org/10.1016/j.sedgeo.2016.02.005

SHERRY, T.J., ROWE, C.D., KIRKPATRICK, J.D., AND BRODSKY, E.E., 2012, Emplacement and dewatering of the world's largest exposed sand injectite complex: Geochemistry, Geophysics, Geosystems, v. 13, p. 1–17. https://doi.org/10.1029/2012GC004157

SPRINKEL, D.A., DOELLING, H.H., KOWALLIS, B.J., WAANDERS, G., AND KUEHNE, P.A., 2011, Early results of a study of Middle Jurassic strata in the Sevier fold and thrust belt, Utah: Utah Geological Association, Publication 40, p. 151–172.

WEIR, G.W., PUFFETT, W.P., AND DODSON, C.L., 1994, Solution-collapse breccia pipes of Spanish Valley, southeastern Utah: U.S. Geological Survey, Open-File Report 94-417, p. 1–33.

WENRICH, K.J., 1985, Mineralization of breccia pipes in northern Arizona: Economic Geology, v. 80, p. 1722–1735. https://doi.org/10.2113/gsecongeo.80.6.1722

WENRICH, K.J., AND HUNTOON, P.W., 1989, Breccia pipes and associated mineralization in the Grand Canyon region, northern Arizona, *in* Elston, D.P., Billingsley, G.H., and Young, R.A., eds., Geology of Grand Canyon, northern Arizona (with Colorado River Guides): Lees Ferry to Pierce Ferry, Arizona: American Geophysical Union, p. 212–218.

WHEATLEY, D.F., CHAN, M.A., AND SPRINKEL, D.A., 2016, Clastic pipe characteristics and distributions throughout the Colorado Plateau: implications for paleoenvironment and paleoseismic controls: Sedimentary Geology, v. 344, p. 20–33. https://doi.org/10.1016/j.sedgeo.2016.03.027

Received 28 May 2017; accepted 26 April 2018.